

**CHARACTERIZATION OF FIXED WIRELESS CHANNELS FOR USE IN
DISTRIBUTION AUTOMATION NETWORKS**

by

Boubacar Diallo

B.A.Sc., The University of Victoria, 2002

A THESIS SUBMITTED IN PARTIAL FULFILLMENT OF
THE REQUIREMENTS FOR THE DEGREE OF

MASTER OF APPLIED SCIENCE

in

THE FACULTY OF GRADUATE STUDIES

(Electrical and Computer Engineering)

THE UNIVERSITY OF BRITISH COLUMBIA

(Vancouver)

April 2011

© Boubacar Diallo, 2011

Abstract

Distribution Automation (DA) is the use of advanced communications network infrastructure in combination with intelligent power equipment and intelligent electronic devices (IEDs) in substations and on distribution feeders to monitor, protect and control the electrical power distribution network. Because wireless networks are generally less expensive, easier to deploy and more resilient than alternatives such as fibre-optic and power line carrier (PLC) networks, they have attracted considerable interest from DA network designers. However, designers must take careful account of the manner in which: 1) the useful range of the links between wireless devices impacts the formation of wireless networks, 2) the depth of fading varies across the range of frequencies available to power utilities for use in such networks, and 3) the degree of shadow fading varies as the height of wireless devices used in such networks rise from pedestrian to pole-top level. Here we show that: 1) the manner in which the distribution assets in BC Hydro's electrical power distribution network are geographically distributed affects the ease with which such assets can be formed into either conventional base-station-to-pole-top fixed wireless macrocell networks or pole-top-to-pole-top fixed wireless mesh networks, 2) the depth of fading experienced on fixed wireless macrocell channels is generally proportional to the carrier frequency and 3) the degree of shadow fading experienced on fixed wireless macrocell channels often increases as the terminal height is raised from pedestrian to pole-top level. These results will help power utilities design reliable and cost-effective wireless networks in support of DA.

Preface

A version of Chapter 2 will be submitted as a contribution to an internal strategy paper concerning Distribution Automation that is currently prepared at BC Hydro. As the lead researcher, I worked closely with Prof. Michelson to formulate the research goals and strategies. I also provided both insights and detailed data concerning BC Hydro's existing electrical distribution system and relevant standards and practices. Soni Upadhyay (undergraduate student) developed the software that we used to analyze the geographic distribution of distribution assets.

A version of Chapter 3 has been published: A. Liou, K. N. Sivertsen, P. Arjmandi, G. Viswanathan, B. Diallo, S. Lancashire and D. G. Michelson, "Characterization of fading on fixed wireless channels between 200 MHz and 2 GHz in suburban macrocell environments," *IEEE Trans. Wireless Commun.*, vol. 8, no. 10, Oct. 2009, pp. 5356-5365. I oversaw installation of the base station facility at BC Hydro's Edmonds facility, provided both insights and detailed information concerning BC Hydro's relevant wireless standards and practices, and worked closely with Prof. Michelson and the other members of the team to formulate the research goals and strategies. In addition: A. Liou, P. Arjmandi and G. Viswanathan configured and calibrated the measurement system, conducted field data collection and data reduction; K. N. Sivertsen conducted MATLAB coding, database maintenance and calibration of equipment and S. Lancashire facilitated access to the BC Hydro site.

A version of Chapter 4 will be submitted for publication. B. Diallo, S. Mashayekhi and D. G. Michelson, "Effect of terminal height on shadow fading of fixed wireless channels at 1.9 GHz in suburban macrocell environments." As the lead researcher, I worked closely with Prof. Michelson to formulate the research goals and strategies. I oversaw field data collection by J. Ku and A. Riyandie (undergraduate students) and reduced the data. S. Mashayekhi used the Wireless InSite software package to generate the simulated data to which we compared the measured data.

Table of Contents

Abstract.....	ii
Preface.....	iii
Table of Contents	iv
List of Tables	vi
List of Figures.....	vii
Acknowledgements	ix
Dedication	x
Chapter 1 Introduction.....	1
1.1 Architecture of the Electric Power Grid.....	1
1.2 Distribution Automation Network Architectures.....	2
1.3 Objectives and Outline.....	4
Chapter 2 The Design of Wireless Networks to Support Distribution Automation.....	6
2.1 Introduction.....	6
2.2 Physical Deployment and Geographic Distribution of DA Assets	7
2.2.1 Description.....	7
2.2.2 Physical Deployment.....	8
2.2.3 Geographic Distribution	10
2.3 Wireless Network Deployment Options for BC Hydro	12
2.4 Discussion	14
2.5 Limitations of Existing Propagation Models	15
2.5.1 Wireless Planning Tools	15
2.5.2 Site-General Models	16
Chapter 3 Characterization of Fading on Fixed Wireless Channels between 200 MHz and 2 GHz in Suburban Macrocell Environments	17
3.1 Introduction.....	17
3.2 The Narrowband Fading Channel Model.....	19
3.3 The Measurement Setup.....	20
3.3.1 The Tri-band Channel Sounder	20

3.3.2	Verification Tool	23
3.3.3	Weather Instrument	23
3.3.4	Test Area.....	24
3.3.5	Data Collection Protocol.....	24
3.4	Results	25
3.4.1	Distribution of Ricean K-factors	25
3.4.2	Path Gain and Ricean K-factors vs. Distance.....	27
3.4.3	Fixed and Scattered Path Gain vs. Distance	28
3.4.4	Excess Path Gain and Ricean K-factor as a Function of Average Wind Speed	30
3.4.5	Excess Fixed Path Gain and Excess Scatter Path Gain as a Function of Average Wind Speed	32
3.4.6	Joint Dependency of the Excess Path Gain and Ricean K-factor	34
3.5	A Simulation Model.....	35
3.6	Conclusions.....	36
Chapter 4 Effect of Terminal Height on Location Variability of Fixed Wireless Channels at 1.9 GHz in Suburban Macrocell Environments		37
4.1	Introduction.....	37
4.2	The Test Site	38
4.3	The Simulator.....	38
4.4	The Measurement Setup.....	39
4.5	Results.....	40
4.5.1	Simulation Results.....	40
4.5.2	Measurement Results.....	42
4.5.2.1	Path Gain vs. Distance	42
4.6	Conclusions.....	45
Chapter 5 Conclusion and Recommendations		46
5.1	Conclusions.....	46
5.2	Recommendation for Future Work	47
References		49

List of Tables

Table 2.1	Minimum standard setting depths.....	9
Table 3.1	Link budget parameters for the tri-band channel sounder.	22

List of Figures

Figure 1.1 - Location variability with different heights of receiving antenna	1
Figure 2.1 - Height distribution of poles.....	9
Figure 2.2 - Geographic distribution of field assets.....	11
Figure 2.3- (a) Count of base stations within 10km range of a device, (b) reduction in the number of orphan devices as base station range is increased, and (c) count of device neighbours within 1km range.....	14
Figure 3.1 - (a) The tri-band transmitter that was deployed at the base station and (b) the tri-band receiver that was carried aboard the propagation measurement van.....	22
Figure 3.2 -Typical time series of received signal strength at 220 MHz (top) and 1900 MHz (bottom) with Ricean K-factors of 24.2 and 7.4 dB, respectively.	25
Figure 3.3 -Distribution of Ricean K-factors observed throughout the test area at (a) 200MHz, (b) 850MHz, and (c) 1900MHz.....	26
Figure 3.4 -Regression analysis of Ricean K-factors vs. carrier frequency in MHz. The distribution of K at 220, 850 and 1900 MHz is indicated by a box plot.....	26
Figure 3.5 - (a) Average path gain G and (b) Ricean K-factors observed at 220 (O), 850 (Δ), and 1900 (\bullet) MHz vs. distance.....	28
Figure 3.6 - (a) Fixed path gain g_f and (b) scattered path gain g_s observed at 220 (O), 850 (Δ), and 1900 (\bullet) MHz vs. distance.....	29
Figure 3.7 - (a) Excess path gain and (b) Ricean K-factors observed at 220 (O), 850 (Δ), and 1900 (\bullet) MHz vs. averaged wind speed.	31
Figure 3.8 -The average wind speed distribution observed at the base station during data collection.....	31
Figure 3.9 - (a) Excess fixed path gain and (b) Excess scattered path gain observed at 220 (O), 850 (Δ), and 1900 (\bullet) MHz vs. average wind speed.....	33
Figure 3.10 -Scatter plots of Ricean K-factor vs. excess path loss at a given distance at (a) 220 (O), (b) 850 (Δ), and (c) 1900 (\bullet) MHz.....	35
Figure 4.1- Clutter hight distribution.....	39
Figure 4.2 - Simulated path gain vs. distance. solid line shows the mean path gain (regression line).....	40

Figure 4.3 - Shadow loss in dB for different distances from transmitter antenna at height h=7m.	40
Figure 4.4 - Shadow loss in dB for receiving antennas at heights of 2, 5 and 7 m.....	41
Figure 4.5 - Location variability with different heights of receiving antenna	42
Figure 4.6 - Average path gain observed at terminal heights of 2, 5 and 7 m vs. distance	43
Figure 4.7- Shadow fading distribution observed throughout the test area at terminal heights of (a) 2 m, (b) 5 m, and (c) 7 m where $\sigma = 5.7, 8.1$ and 8.0 dB, respectively.	44

Acknowledgements

I am grateful to the following organizations for providing both direct and in-kind support to this research project:

- Western Economic Diversification Canada, Bell Canada and British Columbia Hydro and Power Authority (BC Hydro) provided direct financial support for student stipends and equipment acquisition under WD Project 6945.
- BC Hydro provided access to the communications room and the rooftop of their Edmonds facility so that we could set up the base station transmitter that we used during field data collection.
- Bell Canada and TELUS provided access to the 1.8 GHz and 850 MHz radio frequency spectrum, respectively, used during the field data collection.

I express my appreciation my research collaborators listed in the Preface and to my colleagues in the Telecommunications Department of BC Hydro, including Foad Kasiri (Manager), Brian Hills (Specialist Engineer), Sol Lancashire (Telecom Architect) for their ongoing support as I pursued part-time graduate studies.

I owe particular thanks to Prof. David G. Michelson for supervising my work, providing critical guidance, suggestions and consideration, and for being instrumental in my current and future success.

Dedication

To my parents and my sisters (Souadou, Asmaou and Zeinabou Diallo) who have supported me throughout my years of education.

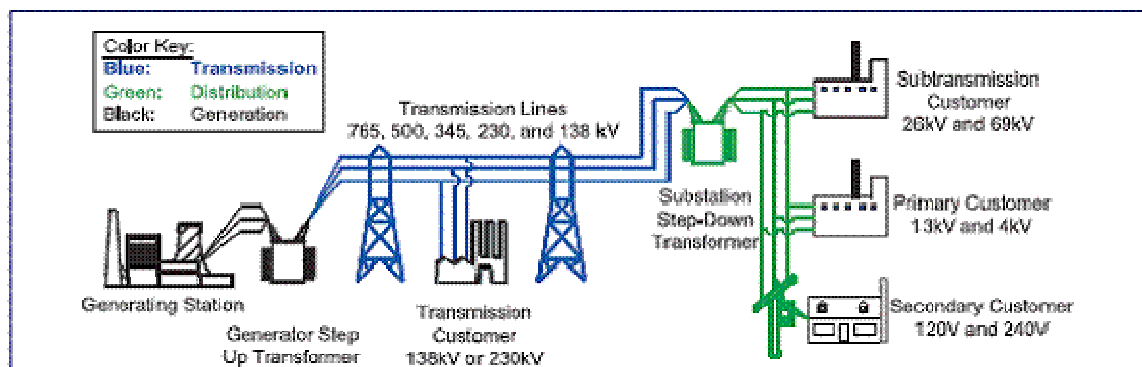
Chapter 1

Introduction

This thesis is concerned with the application of wireless communication networks to automation of the electrical power distribution grid. In particular, it is concerned with the manner in which: 1) the useful range of the links between wireless devices impacts the formation of wireless networks, 2) the depth of fading varies across the range of frequencies available to power utilities for use in such networks, and 3) the degree of shadow fading varies as the height of wireless devices used in such networks rise from pedestrian to pole-top level. The results presented here will help power utilities design reliable and cost-effective wireless communication networks that support Distribution Automation (DA).

1.1 Architecture of the Electric Power Grid

The electric power grid has traditionally been divided into generation, transmission and distribution portions, as suggested by Fig. 1.1. Power flow is radial and originates from generating stations. The power is stepped up to a higher voltage and transported over high voltage transmission lines. The generating stations and high voltage transmission lines are collectively referred to as the bulk power system. After the power reaches a substation, the voltage is further stepped down and supplied to customers through a distribution grid.



Source: www.nerc.com

Figure 1.1 – The current electrical power grid

Electric power utilities in North America (USA, Canada and a portion of Baja California in Mexico) have chosen to interconnect their bulk power systems in order to provide both flexibility and redundancy. The need to develop and enforce standards for the reliable

operation of such a vast network led to the formation of the North American Electric Reliability Corporation (NERC) in 1968. U.S.-based entities that are found to be in violation of a NERC standard may be fined of up to US\$1 million per day per violation.

In order to support operation of their bulk power systems and be compliant with NERC standards, electric power utilities throughout North America have made a considerable investment in highly robust and highly engineered point-to-point microwave and fiber optic communication networks. The relatively small number of sites and field equipment in the bulk power system that must be interconnected has eased the task of deploying and maintaining such a network. By contrast, the distribution grid has orders of magnitude more sites and field equipment and the reliability of individual elements is inherently less critical to the operation of the overall system. This has historically made it difficult to justify the cost of deploying wide area communication networks to support Distribution Automation.

In recent years, the electrical power industry has begun to: 1) promote independent and renewable power production, 2) develop new power system architectures such as microgrids and 3) work toward increasing system reliability and power quality in the face of increasing demand. In 2007, this led the U.S. Department of Energy to announce a major initiative to modernize the electric power distribution grid and deploy smart metering and distribution automation networks under the moniker Smart Grid [2]. Regulators around the world have subsequently announced similar initiatives [3] [4]. The Government of British Columbia has mandated the replacement of 1.8 million existing electrical meters in the province with smart meters by 2012 [5]. BC Hydro expects to start deploying distribution automation networks shortly thereafter. In doing so, they plan to leverage the communication infrastructure that has been established for the smart metering program.

1.2 Distribution Automation Network Architectures

Numerous configurations and architectures for Distribution Automation networks have been proposed. The U.S National Institute of Standards and Technology (NIST) and the International Electrotechnical Commission (IEC) have developed frameworks and action plans that will address communication interoperability between the various advanced communication architectures and configurations [6],[7]. Several industry task forces and standards organizations such as Open Smart Grid (OpenSG) and the Institute of Electrical and Electronics Engineers Project 2030 Task Force 3 (IEEE P2030 TF3) are developing

system requirements and architectures for the implementation of these action plans. OpenSG's main task is to provide system requirements specification for Smart Grid communication [8] while IEEE P2030 TF3 is actively working on the development of guidelines for Smart Grid intersystem and subsystem communication interoperability [9]. However, the current efforts initiated by NIST and IEC have paid scant attention to the physical deployment of wireless network devices or the propagation characteristics of the links between such devices.

Wireless networks are expected to play an important role in DA strategy because they are generally less expensive, easier to deploy and more resilient than alternatives such as fiber-optic and power line carrier networks. To further promote the use of wireless networks for DA, spectrum regulators have recently begun to reallocate frequency bands below 2 GHz for use by electrical power utilities [10],[11],[12]. Electrical power utilities have two principal options for the deployment of their DA wireless networks: 1) Point-to-multipoint macrocell networks in which a base station located above rooftop level communicates with several DA devices located at pole-top level over ranges of up to 10 km, and 2) pole-top-to-pole-top mesh networks in which DA devices communicate directly with each other over distances of up to 1 km.

Previous studies of the use of wireless networks for distribution automation have focused mostly on the architecture of and information flow within such networks. Scant attention has been paid to physical deployment of the wireless devices within such networks or the manner in which the useful range of the links between wireless devices impacts the formation of DA networks. Over the years, propagation models have been developed to characterize the manner in which path loss, or its reciprocal, path gain, is affected by the carrier frequency, the heights of and separation between the base station and mobile terminal in suburban macrocell environments [13],[14],[15]. However, these channel models don't address key issues that are crucial for a reliable wireless network deployment for DA applications, including 1) depth of signal fading on fixed wireless channels, and 2) effect of terminal height on the location variability experienced on fixed wireless macrocell channels. This places those responsible with the simulation, planning and design of such systems at a severe disadvantage when asked to predict system coverage and outage probabilities. As a result, there is a risk of either 1) overdesigning the wireless networks and incurring higher

capital costs and lower return on investment or 2) under-designing the wireless networks and incurring decreased reliability and throughput and possibly requiring costly redesign.

1.3 Objectives and Outline

The objectives of this thesis are: 1) to determine how the manner in which the DA assets in BC Hydro's distribution system are geographically clustered affects the ease with which such assets can be formed into either conventional base-station-to-pole-top macrocell networks or pole-top-to-pole-top mesh networks, 2) to characterize the depth of fading on fixed wireless macrocell channels and its implications for DA, and 3) to characterize the effect of terminal height on the location variability experienced on fixed wireless macrocell channels and its implications for Distribution Automation, and 4) to identify any unresolved issues for future research studies.

This thesis is organized as follows: In Chapter 2, we assess the geographical distribution of the distribution assets of BC Hydro by collecting Geographic Information System (GIS) data of the field equipment and potential base stations. The data is classified into clusters through numerical analysis. From the results, we characterize the physical deployment scenarios for BC Hydro DA. Queries from the data are then used to assess the ease in which the assets can be formed into point to multipoint and into poletop-to-poletop wireless network options.

In Chapter 3, we address the second objective by collecting time-series received signal strengths at 84 fixed locations at ranges between 1 and 4 km from the base station. The measurement campaign was conducted in a typical suburban macrocell environment. The clutter was mainly made up of light to moderate foliage and one-and two-storey houses. After numerical analysis of the data, we characterize the signal fading in such macrocell environment.

In Chapter 4, we address the third objective by conducting a set of 1.9 GHz experiments in the same suburban macrocell environment as the one used in Chapter 3. We measured time-series received signal strengths at 80 fixed locations and three different remote terminal heights at ranges between 1km to 3km. We generated a collective database from which we could construct the distribution of location variability experienced on such environments at different heights.

Finally in Chapter 5, we draw conclusions, assess the contributions and limitations of the work, and recommend future work.

Chapter 2

The Design of Wireless Networks to Support Distribution Automation

2.1 Introduction

Distribution Automation (DA) is the use of advanced communication network infrastructure in combination with intelligent power equipment and Intelligent Electronic Devices (IEDs) installed in substations and on distribution feeders to monitor, protect and control the electrical distribution network [19], [20]. Initially, the major distribution field equipment (reclosers, voltage regulators, switches, capacitor banks, transformers, sectionalizer, etc...) were conceived and designed to work independently and performed basic pre-programmed functions. With the introduction of Distribution Automation, these devices can now be remotely controlled through different communication links [21], [22].

The automation of the aging distribution network is essential in order to achieve a reliable supply, high power quality, increase environmental responsibility, and greater customer satisfaction. Utilities have considered distribution automation since the early 80's [23],[24]. However, most past attempts of distribution automation involved small pilot projects to assess the added value of integrating intelligence to various applications of the distribution network [25]-[28]. This lack of distribution automation is explained by 1) the difficulty of utilities to justify the cost associated with such a large scale network deployment to the regulators and stakeholders, and 2) the non existence of adequate standards.

In 2007, the U.S Department of Energy announced a major effort to modernize the electric power distribution network [2]. This effort coupled with the advances and falling prices of the communication and control technologies had led most utilities including BC Hydro to develop Distribution Automation strategies which aim at identifying gaps in the protection, control and monitoring of the existing infrastructure and providing a roadmap that will address these gaps.

Distribution Automation is not possible without ubiquitous communication to the controllable devices. Wireless networks are expected to play an important role in Distribution Automation strategy because such networks are generally less expensive, easier to deploy and more resilient than alternatives such as fiber-optic and power line carrier networks. However, careful account must be taken of the manner in which propagation impairments

restrict the useful range of the wireless links used in such networks. Most previous and present work has focused on network architecture and functional requirements of the distribution automation communication infrastructure rather than the details of physical deployment and wireless coverage [6]-[9].

In order to properly formulate the wireless communications aspects of their Distribution Automation strategy, BC Hydro must consider: 1) The manner in which Distribution Automation assets are physically deployed and geographically clustered, 2) How this affects the ease with which DA assets can be formed into either conventional base-station-to-pole-top macrocell networks or pole-top to pole-top mesh networks, 3) The limitations of existing RF coverage prediction techniques.

The objectives of this work are 1) to consider several of the above-mentioned issues, 2) assess the remaining issues, and 3) recommend next steps. This chapter is outlined as follows: In Section 2, we classify BC Hydro's distribution field equipment based on Geographic Information System (GIS) data collected. In Section 3, we consider the ease with which the collected GIS data can be formed into either macrocell networks or poletop to poletop mesh networks. In Section 4, we draw conclusions, and recommend future work.

2.2 Physical Deployment and Geographic Distribution of DA Assets

2.2.1 Description

A variety of equipment will require two-way communications under the Distribution Automation scenario. However, we have focused our attention on three types of equipment based on their significance and plans to extend DA to them in the near future: reclosers, voltage regulators and capacitor banks.

A *recloser* is a self-contained device with the necessary intelligence to sense overcurrents and time, to interrupt the overcurrent, and to reclose automatically to re-energize the line. If the fault is permanent, the recloser will lock open (lock out) after a preset number of operations and thus isolate the faulted section from the main part of the system, reducing the effect of the fault on the system. Reclosers communicate with the Distribution Management System in feeder reconfiguration application where the system automatically reconfigures feeders to restore service to downstream portions of a faulted feeder. They also

send status data to the Distribution Management System (DMS) and receive configuration data from it.

A *voltage regulator* is used to boost or buck the distribution system voltage to maintain the nominal voltage at service entrances and points of electricity utilization within specified Canadian Standard Association limits under all loading and operating conditions [29]. Voltage regulators are equipped with controllers that receive control signals from the Distribution Management System. The voltage regulators change the voltage settings based on the received control signals and the local measurements (load, voltage, etc...). Besides performing the basic voltage regulating functions, the controllers provide real time and historical information about the voltage regulators used for scheduled maintenance and life expectancy of the regulator. The controllers also send status data to the DMS and receive configuration data from the DMS.

A *switched capacitor bank* is primarily used to provide a fixed source of reactive power (VARs) when needed to compensate for inductive customer loads (motors, etc...). Switched capacitor bank controllers determine whether the associated capacitor bank should be switched on or off based on local measurements (Voltage, VAR, time, temperature, etc...) and/or remote control signals from the Distribution Management System.

2.2.2 Physical Deployment

Over 95% of the field equipment Distribution Automation assets is located on BC Hydro owned distribution poles. The common pole lengths used for BC Hydro distribution lines and services are 9.1m, 10.6m, 12.2m, 13.7m, 15.2m, and 16.7m [30]. These poles must be buried with minimum standard setting depths in order to provide sufficient overturning resistances to counteract the expected wind force. The minimum depths vary depending on whether the ground is soil or rock. The minimum depths for soil (which are higher than for rock) are given in Table 2.1[30]. The height distribution of these poles is shown in Fig. 2.1. Pole heights of 11.7m and 10.4m are the most used and account for 45% and 31% respectively of the total number of poles in the specified range.

Table 2.1 Minimum standard setting depths.

Pole lengths (m)	Depth in soil (m)	Pole heights (m)
9.1	1.5	7.6
10.6	1.7	8.9
12.2	1.8	10.4
13.7	2	11.7
15.2	2.1	13.1
16.7	2.3	14.4

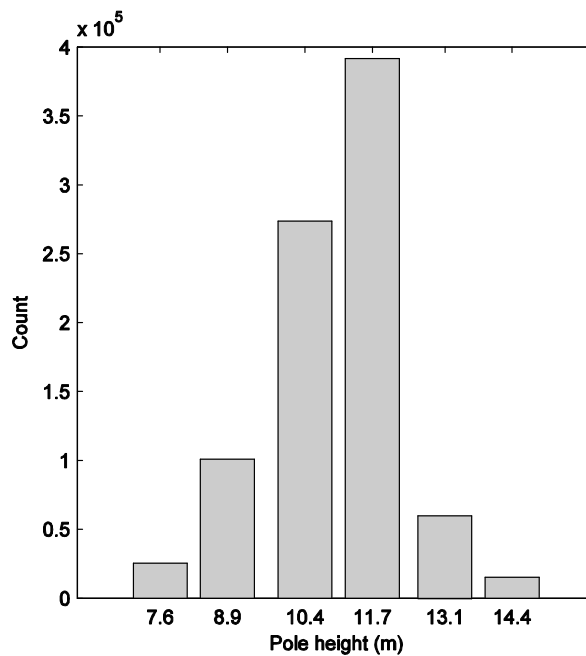


Figure 2.1 – Height distribution of poles

BC Hydro has specific standards regarding the location of the field Distribution Automation assets on distribution poles in order to: 1) provide uniform operating practices, 2) effect efficient quality control and inspection, and 3) ensure uniform safety requirements comply with B.C Regulations. The field equipment is mounted above the neutral conductor. The neutral is normally placed at a minimum height of 2m below the primary phase conductors in

order to 1) allow for present and future space requirements for the installation of the various field equipment configurations, and 2) allow adequate space for a certified utility arborist to drive a tree-trimming bucket between the primary and neutral conductors such that the maneuver can be safely performed in compliance with the B.C Occupational Health and Safety Regulation [30]. In most cases, the reclosers are located at 3m above ground, the voltage regulators at 6 and 8 m and the capacitor banks at 5 and 7m.

Any installation of communication equipment on distribution poles also follows specified standards which limits the height of the communication equipment to 1m below the neutral [30]. This ensures safety clearance from live lines for people who will be working with this equipment [31]. Also this simplifies the installation of the equipment as no specialized qualification is required. Although the height requirements of the communication equipment and field devices are restricted, the analysis for the planning of the deployment of wireless network for Distribution Automation is simplified since we only need to consider a limited, well defined range of terminal heights.

2.2.3 Geographic Distribution

The successful deployment of any wireless network requires useful insights into the geographic distribution of the assets. We collected Geographic Information System (GIS) data of BC Hydro's existing pole-top reclosers, voltage regulators and capacitor banks which totalled 1335. BC Hydro has partitioned its distribution network into 8 geographical areas. The distribution of the field equipment among these areas and the proportion of the total field equipment installed in each area are shown in Table 2.2. The geographic distribution of the field equipment is shown in Figure 2.2. It is apparent from the data that Fraser Valley, Metro Vancouver and Vancouver Island account for half of the installed field equipment. These regions represent the most populous areas where the bulk of the load is concentrated. We also collected Geographic Information System (GIS) data of BC Hydro existing microwave repeater sites and substations which totalled 335. Given the large number of assets involved and their geographic distribution, we need to develop a systematic way for assessing and planning wireless distribution automation networks.

Table 2.2 Field equipment asset data

Area	Voltage Regulators	Reclosers	Capacitor banks	Proportion of total field equipment
Central	27	50	18	7.11%
Northern	57	92	30	13.4%
Okanagan	26	90	7	9.21%
Thompson Shuswap	50	170	25	18.35%
Fraser Valley	10	83	170	19.7%
Metro Vancouver	20	50	109	13.41%
Vancouver Island	32	65	154	18.8%
Total	222	600	513	

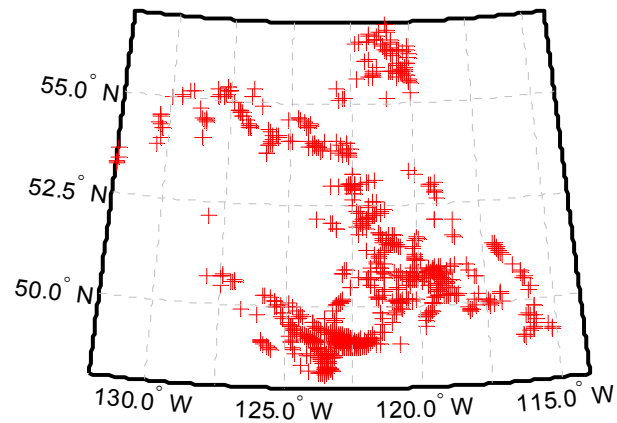


Figure 2.2 – Geographic distribution of field assets

2.3 Wireless Network Deployment Options for BC Hydro

Wireless network deployments for Distribution Automation fit into two categories 1) A private wireless network where the utility deploys and owns the assets of the wireless network, and 2) A public wireless network where the utility relies on external communication service providers. The public wireless network consists of cellular or satellite technologies. Utilities are generally reluctant to deploy a public wireless network for their mission critical applications such as Distribution Automation due to the inadequate latency, security, and reliability requirements of such network. Hence the deployment strategy of choice tends to be private wireless network that has two predominant technologies

1) The Worldwide Interoperability for Microwave Access, or WiMAX based on IEEE 802.16d standard, is a wireless solution for extending broadband access over longer distances[32],[33]. WiMAX is an attractive solution for a number of reasons including 1) WiMAX is standard-based technology, 2) the technology is interoperable which means that utilities can source their equipment from multiple vendors and select the best for each application, 3) WiMAX has low latency (<100ms), high security, wide coverage and high capacity which are paramount to the utility sector

WiMAX based on IEEE 802.16d standard is a point to multipoint solution where a base station communicates with field equipment in the coverage area. The WiMAX solution can be closely modeled as conventional base station-to-pole-top macrocell networks

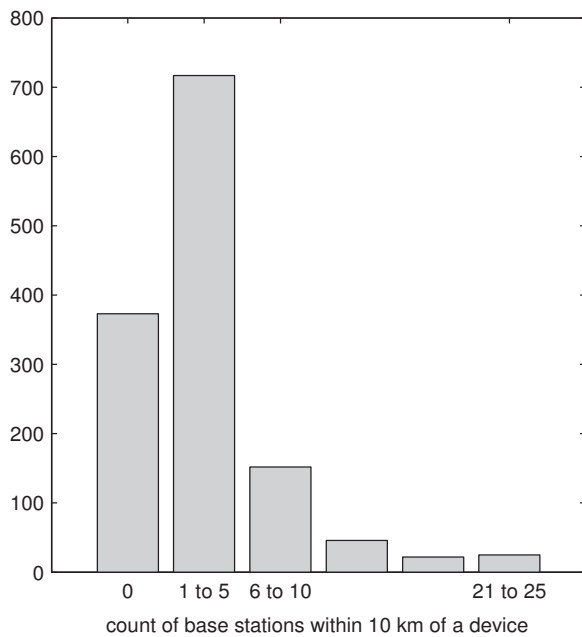
2) Zigbee, a suite of high level communication protocols, uses the IEEE 802.15.4g global standard to provide low rate wireless mesh networking[35],[36]. IEEE 802.15.4g was developed to provide a global standard to facilitate very large scale process control applications such as Distribution Automation. Zigbee based on IEEE 802.15.4g is an attractive solution for a number of reasons including 1) It is a standard based technology, 2) high reliability, and 2) low cost allows the technology to be widely deployed.

Zigbee based on IEEE 802.15.4.g standard is a mesh solution where the field equipment communicates directly with each other. This solution can be closely modeled as pole-top to pole-top mesh networks

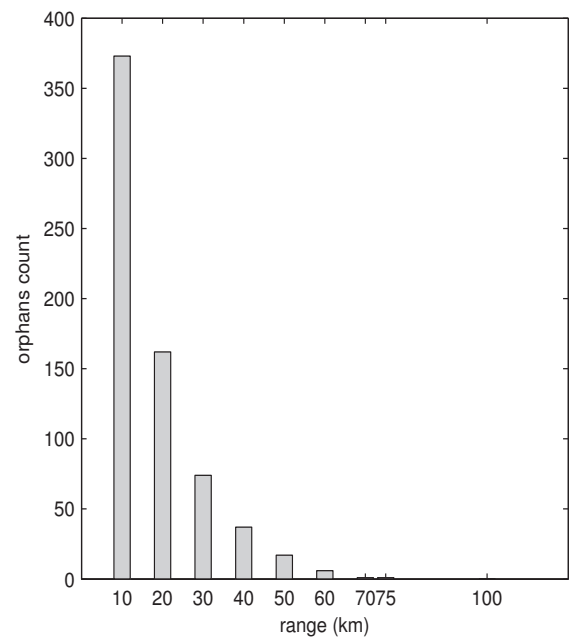
Our objective is to assess the ease in which the distribution assets described in Section 2.2 can be formed into either conventional base-station-to-pole-top macrocell networks based on the WiMAX technology or pole-top-to-pole-top mesh network based on the Zigbee

technology. Our starting point for this assessment is the GIS data of the assets described in Section 2. We query the base stations that are within a 10 km range of a field equipment device for the macrocell network scenario to determine the coverage area of the existing base stations. A range of 10 km corresponds to the typical threshold point of the WiMAX Customer Premise Equipment radio based on our assumptions of free space loss over plane earth. For the mesh network, we query a neighbour count for each device within 1 km range of that device. A range of 1 km corresponds to the typical threshold point of the Zigbee based terminal radio based on our assumptions of free space loss over plane earth. Our method is a useful tool for providing insight to those charged with wireless network deployment strategies for Distribution Automation. It gives a reasonable estimate to a complex problem before turning to more sophisticated methods to calculate a precise answer.

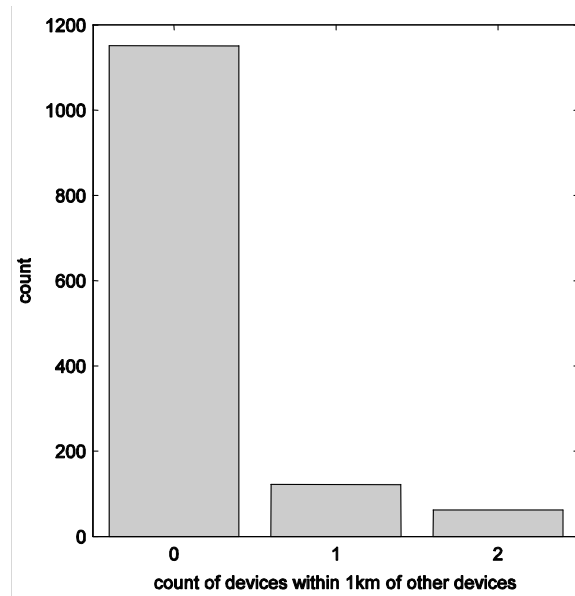
The results of our queries are presented in Figure 2.3-2.5. We found that 27% of the field equipment devices (count of 373 devices) which we refer to as “orphans” don’t have communication to a base station. Increasing the range of the base stations from 10 km to some higher number shows that doubling or even tripling the range to 20 or 30 km will dramatically reduce the number of orphans.



(a)



(b)



(c)

Figure 2.3 – (a) Count of base stations within 10km range of a device, (b) reduction in the number of orphan devices as base station range is increased, and (c) count of device neighbours within 1 km range

2.4 Discussion

Decisions concerning the best ways to deploy wireless networks for Distribution Automation are based on availability of links between wireless nodes and between wireless nodes and potential base station locations. This is a particularly significant issue for BC Hydro given that its DA assets are widely dispersed across the province.

We have conducted a preliminary assessment of the wireless connectivity options of BC Hydro's 1335 field equipment assets that are currently deployed. Our findings are summarized as follows:

- Mesh networks based upon Zigbee wireless technology are not a viable method for interconnecting BC Hydro's distribution assets given that few assets have at least one neighbour within a range of 1 km.
- Wide area networks based upon WiMAX wireless technology can cover almost 75% of BC Hydro's assets from existing BC Hydro substations and repeater sites.

Extending coverage to all sites will require additional base stations at non BC Hydro sites.

After suitable modification, automatic approaches to optimum base station site selection for cellular systems may be useful in planning DA deployments. The details remain an open research question.

The deployment of Distribution Automation wireless networks requires adequate propagation models so that link budgets can be adequately estimated. Site general propagation models for pole-top to pole-top within a 1-km range are currently not available and should be developed soon to facilitate large-scale deployment of mesh networks based upon Zigbee wireless technology.

Site general models for wide area networks based upon WiMax wireless technology do not address two main key issues specific to the deployment of wireless networks for Distribution automation 1) depth of signal fading below 2 GHz, and 2) effect of terminal height on signal location variability. These two main issues will be discussed in chapters 3 and 4 respectively.

2.5 Limitations of Existing Propagation Models

Propagation models are required for the planning, design, deployment, and testing of wireless networks for Distribution Automation. Propagation models can be developed from wireless planning tools or through measurement of the environments.

2.5.1 Wireless Planning Tools

Wireless Planning tools make use of sophisticated computer aided numerical analysis to perform detailed coverage studies. Although this method is one of the most accurate methods, it requires tremendous amount of detailed data regarding the type and location of each clutter in the entire region of interest.

The wireless planning tool option is not usually the first choice because 1) the required clutter data is very costly, 2) the process is very time consuming, and 3) the level of details and accuracy produced by wireless planning tools are not required for the purpose of coverage studies.

2.5.2 Site-General Models

A reasonable approach of developing propagation models is to use site-general propagation models which are measurement based models that broadly capture the scenarios in which the wireless links will be deployed.

Site general macrocell propagation models have been studied extensively over the last decades. The most noticeable ones are 1) the Hata-Okumura model which is valid in the frequency range of 500 to 1500 MHz and base station heights above 30 meters with user distances greater than 1 km [13], 2) the Cost 231 model which extends the Hata-Okumura model to 2 GHz [14], and 3) the AT&T model which is the ultimate extension to the Hata-Okumura model that takes into account the new communication systems (Personal Communications Services, Multipoint Distribution Services) that tend to operate at higher frequencies with shorter base station heights and smaller cells [15].

However the AT&T model does not account for 1) depth of fading as a function of frequency, 2) effect of terminal height on signal location variability, and 3) pole-top to pole-top communication scenarios.

The issues in 1) and 2) are addressed in chapters 3 and 4 respectively. We have not addressed pole-top to pole-top communication in this thesis

Chapter 3

Characterization of Fading on Fixed Wireless Channels between 200 MHz and 2 GHz in Suburban Macrocell Environments

3.1 Introduction

Fixed wireless technology has attracted considerable interest in recent years as: 1) common carriers seek methods for providing either fixed or nomadic network access services to residential households without the expense of deploying wireline connectivity over the last mile [36],[37], and 2) as public utilities seek methods that will allow them to: (a) detect and report outages, (b) monitor usage, and (c) implement strategies that encourage customers to limit consumption and adopt sustainable practices [20],[38],[39]. In suburban macrocell environments, *i.e.*, environments in which the base station antenna is mounted well above the local rooftop or treetop level and the remote terminal antenna is mounted below the local rooftop or treetop level, wireless links are usually obstructed by intervening obstacles and a large fraction of the signal that reaches the receiver does so as a result of scattering and diffraction by objects in the environment. Because both the transmitting and receiving antennas in such applications are fixed, solely the motion of objects in the environment that scatter and diffract the signal causes signal fading. In suburban macrocell environments, a large fraction of those objects are trees and foliage with leaves and branches that sway when blown by the wind.

During the past decade, groups in Canada, the United States, the United Kingdom, Chile, Australia and elsewhere have conducted measurement campaigns aimed at characterizing the manner in which signal fading occurs on non-line-of-sight (NLOS) paths in macrocell environments, *e.g.*, [40]-[47]. Such studies have variously sought to characterize: 1) the first-order statistics of the fading signal envelope over time and location, 2) the rate at which the signal fades, either through direct estimation of the Doppler spectrum or through estimation of the average fade duration and level crossing rate, 3) the effect of the height and beamwidth of the receiving antenna, local density of vegetation and the wind speed in the vicinity, and 4) the performance of space and polarization diversity at either the base station or the remote terminal.

The vast majority of previous studies of fixed wireless channels in suburban macrocell environments focused on individual frequency bands at 1.9 GHz and above, including the PCS band at 1.9 GHz, the ISM band at 2.45 GHz, the Fixed Wireless Access (FWA) band at 3.5 GHz and the U-NII and ISM bands at 5.2 and 5.8 GHz. However, spectrum regulators have recently begun to reallocate frequency bands below 2 GHz in order to help meet the requirements for broadband wireless access for urban and rural areas and/or narrowband telemetry for public utilities. In Canada, spectrum in frequency bands near 700 MHz has been proposed for fixed wireless broadband use in rural areas [12] and may find application in distribution automation by the electrical power industry. Frequency bands such as 220–222 MHz and 1429.5–1432 MHz have recently been designated for utility telemetry and distribution automation [48]. Regulators are increasingly designating multiple primary allocations within individual frequency bands, as well as proposing more flexible licensing schemes, in an attempt to accommodate different users and services in the same spectrum. Both the amount of radio spectrum, and the choice of frequency bands available for fixed wireless use, will almost certainly increase in coming years.

The manner in which path loss, or its reciprocal, path gain is affected by the carrier frequency, the heights of and separation between the base station and mobile terminal in suburban macrocell environments over the range from 200 MHz to 2 GHz has been well-studied over the years and has been captured by several standard models[13]-[15]. However, existing channel models do not provide a description of the depth of signal fading that fixed wireless channels will experience over this frequency range in suburban macrocell environments. (Ref. [49] describes fading on UHF links between fixed nodes within a tropical rain forest but the link configuration (both nodes were located below the forest canopy) was quite different from that encountered in suburban macrocells.) This lack of information places those charged with planning, simulating or deploying fixed wireless systems in suburban macrocell environments at a severe disadvantage when asked to predict system coverage and outage probabilities.

Here, we take the first steps to develop measurement-based fading channel models suitable for use across the frequency range from 200 MHz to 2 GHz. We established a transmitting site atop an eighteen-storey office tower located in the middle of a large suburban area. We simultaneously broadcast single carrier signals in the 220, 850 and 1900

MHz bands and collected time-series of the received signal strength observed in each band at fixed locations at ranges between 1 and 4 km. We reduced the data in order to determine the manner in which path gain and signal fading vary with distance, time-averaged wind speed and carrier frequency in a typical suburban macrocell environment. The resulting measurement-based model allows the coverage and outage probability in a typical macrocell environment to be compared. The frequencies that we employed bracket the majority of the bands that have been allocated to electric power utilities for fixed wireless access and SCADA (supervisory control and data acquisition) applications. Although our results strictly apply to narrowband channels, they are also relevant to single carriers in multicarrier modulation schemes. The results presented here are specific to high transmitting sites; in future work, we shall determine how lowering the base station height affects the results.

3.2 The Narrowband Fading Channel Model

The essential aspects of fading on narrowband fixed wireless channels have been described previously in [40],[41] and[50]. The complex signal path gain of a narrowband channel (typically tens of kHz wide) over a given time interval (typically several minutes long) is given by

$$g(t) = V + v(t), \quad (3.1)$$

where V is a complex number and $v(t)$ is a complex, zero-mean random time variation caused by windblown foliage, vehicular traffic, *etc.* Both V and the parameters of the random process $v(t)$ may change from one time-frequency segment to another.

From time series data collected over a given time-frequency segment, we can calculate the average power gain

$$G = \overline{|g(t)|^2} = |V|^2 + \overline{|v(t)|^2} = |V|^2 + \sigma^2, \quad (3.2)$$

where σ^2 is the variance of the complex Gaussian process. The rms fluctuation of the envelope about the mean is given by the standard deviation of $|g(t)|^2$ and is denoted by σ_G . Because experience has shown that $v(t)$ is a complex Gaussian process, the distribution of $|g(t)|^2$ over time is Ricean. The K-factor of the distribution is given by

$$K = |V|^2 / \overline{|v(t)|^2} = |V|^2 / \sigma^2. \quad (3.3)$$

Various methods for estimating K have been proposed; we use the moment-based method described in [50] where

$$K = \frac{|V|^2}{\sigma^2} = \frac{\sqrt{G^2 - \sigma_G^2}}{G - \sqrt{G^2 - \sigma_G^2}}. \quad (3.4)$$

In terms of G and K , the expression for $g(t)$ in (3.1) can be re-cast as

$$g(t) = \sqrt{\frac{G}{K+1}} \left[\sqrt{K} e^{j\Psi} + x(t) \right], \quad (3.5)$$

where Ψ is the phase of V and $x(t)$ is a zero-mean complex Gaussian process with a unit standard deviation. From (3.5), the channel parameters G and K completely specify the first-order statistics of the signal at a given location over time intervals of several minutes.

Knowledge of the first order statistics of signal fading is sufficient to predict the probability of the link experiencing a given fade depth or outage. Further, it has been observed that the level of cross-polar discrimination (XPD) on the channel is highly correlated with Ricean K-factor [51]. Previous measurements in suburban macrocell environments at frequencies above 1.5 GHz have shown that on Ricean channels, G and K are both well-modeled by Gaussian distributions when they are expressed in dB, *e.g.*, [40]. The implication of this result is that these parameters can be modeled and simulated as a set of Gaussian variates whose joint distribution is completely determined by their means, standard deviations and mutual correlation coefficients. In the sections that follow, we describe our efforts to characterize the parameters of this first-order model in a typical suburban macrocell.

3.3 The Measurement Setup

3.3.1 The Tri-band Channel Sounder

Our tri-band channel sounder consists of a multiband continuous wave (CW) transmitter and receiver that operate in the 220, 850 and 1900 MHz frequency bands. A block diagram of the CW transmitter is shown in Figure 3.1(a). The signal source portion of the transmitter contains a pair of Marconi 2022 RF signal generators, each of which is capable of supplying a CW signal up to 6 dBm over the range 10 kHz to 1 GHz, and a Marconi 2031 RF signal generator capable of supplying a CW signal up to 13 dBm over the range 10 kHz to 2.7 GHz. The signal generators are locked to a 10 MHz reference signal supplied by a Stanford

Research Systems PRS10 Rubidium frequency standard. It, in turn, is disciplined by the 1 PPS signal supplied by a Trimble Resolution-T GPS receiver that has been designed for such applications.

The amplifier portion contains three power amplifiers: 1) a TPL Communications LMS series RF power amplifier capable of delivering between 20 and 100 W at 220 MHz, 2) a Unity Wireless Dragon RF power amplifier capable of delivering up to 30 W between 869 and 894 MHz and 3) a Unity Wireless Grizzly RF power amplifier capable of delivering up to 35 W between 1930 and 1990 MHz. During data collection, all three amplifiers were configured to deliver 20 W signals to their respective feedlines. A wireless remote control device that operates near 150 MHz allowed the data collection team to remotely enable or disable the power amplifiers at the start or end of a measurement session. The 220, 850 and 1900 MHz transmitting antennas are omnidirectional and have gains of 8.1, 6.1 and 5.0 dBi, respectively. They were installed atop the eighteen-storey office tower at BC Hydro's Edmonds facility in Burnaby, BC at a height of 80 m above ground level. The remaining parameters used in the system link budget for each band are given in Table 3.1.

A block diagram of our multiband receiver is shown in Figure 3.1(b). The receiving antennas are omnidirectional and all have the same nominal gain of 1 dBi. When used in NLOS configurations, fixed wireless antennas are typically mounted at heights between 0.5 m (*e.g.*, for nomadic applications) and 4 m (*e.g.*, for permanent installations). As a compromise, we mounted the antennas on the roof of our propagation measurement van at a height of 2.3 m. In many cases, fixed wireless antennas are directional. Because our primary objective is to compare the behaviour of the channel at different frequencies, we elected to simplify the data collection protocol by collecting the measurement data using omnidirectional antennas. If the remote terminal antenna's beamwidth decreased or its height is increased, the path gain and/or the Ricean K-factor will tend to increase [41].

Table 3.1 Link Budget Parameters for the Tri-band Channel Sounder.

Parameter	220 MHz	850 MHz	1900 MHz
Transmitted Power	43 dBm	43 dBm	43 dBm
Transmit Cable Loss	1.3 dB	2.7 dB	4.3 dB
Transmit Antenna Gain	8.1 dBi	6.1 dBi	5 dBi
Receive Antenna Gain	1 dBi	1 dBi	1 dBi
Receive Cable Loss	0.37 dB	0.76 dB	1.2 dB
Receiver LNA Gain	-	30 dB	26 dB

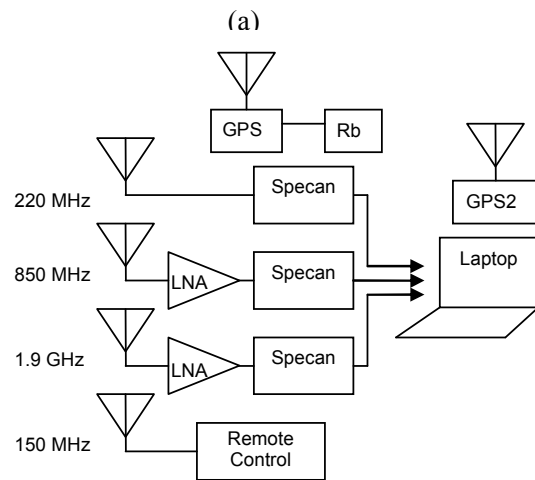
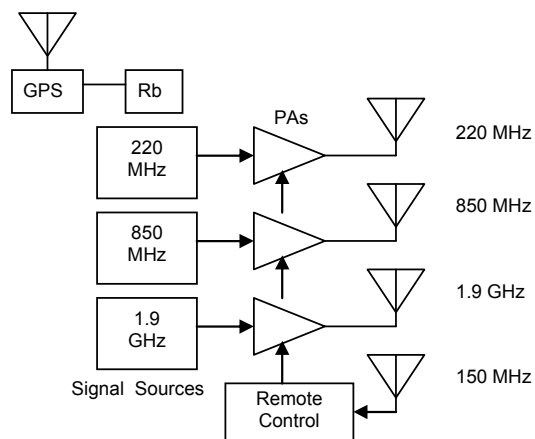


Figure 3.1 (a) The tri-band transmitter that was deployed at the base station and (b) the tri-band receiver that was carried aboard the propagation measurement van.

The multiband receiver consists of: 1) a pair of Anritsu MS2651B spectrum analyzers that operate over the range of 9 kHz to 3 GHz with a selectable IF bandwidth, 2) an Anritsu

MS2721A spectrum analyzer that operates over the range of 100 kHz to 7.1 GHz with a selectable IF bandwidth, 3) a Stanford Research Systems PRS10 Rubidium frequency standard that generates a 10 MHz reference signal to which the spectrum analyzers can be locked and 4) a Trimble Resolution-T GPS receiver that supplies the 1 PPS signal used to discipline the frequency standard. External low-noise pre-amplifiers with 30 dB and 26 dB gain were used to increase the sensitivity of the spectrum analyzers that measure the received strength of the 850 and 1900 MHz signals, respectively. We used a laptop computer equipped with a GPIB adapter to: 1) configure the spectrum analyzers and 2) collect data from them. We geocoded the data with a nominal circular error probability (CEP) of less than 5 metres using location information supplied by a u-blox Antaris 4 SuperSense GPS receiver.

3.3.2 Verification Tool

Before we collected any field data, we verified the function and operation of our tri-band CW channel sounder using a Spirent SR5500 channel emulator. We set the relevant narrowband channel parameters, including path gain and Ricean K-factor, to various values over a broad range and, in each case, confirmed that we were able to correctly estimate each of the parameters. We verified the transmitted power levels using a Bird Model 5000EX digital wattmeter.

3.3.3 Weather Instrument

We measured the wind speed, wind direction, rain rate and outdoor temperature using a Davis Vantage Pro 2 wireless weather station that we mounted on a mast located about 30 metres away from the transmitting antennas. Internally, the weather station samples the relevant weather parameters every few seconds. Once per minute, it logs the average values of these parameters over the previous minute to an internal database. We used a custom software tool to match the received signal strength data collected at a given location to the relevant weather data. Because previous work has shown that variations in average wind speed at tree top level or above are well correlated over mesoscale distances of several kilometers [52], we concluded that collecting wind data at a single location near the base station would be adequate for our purposes.

3.3.4 Test Area

Our test area consisted of suburban neighbourhoods with generally flat terrain, light to moderate foliage and one- and two-storey houses. We collected measurement data at 84 fixed measurement locations that were situated within an annulus between 1 and 4 km from the transmitter site. Almost all the motion in the environment arose from windblown foliage; few, if any, cars, people or other moving scatterers were in the vicinity when we collected measurement data. Most of the foliage in the area is deciduous and between 4 and 7 m in height but at least one-third is coniferous and up to 15 m in height. The duration of the measurement campaign was too short to permit observation of the effects of seasonal variations in the foliage. All of our data was collected with leaves on the trees.

3.3.5 Data Collection Protocol

Our data collection protocol comprised the following steps. First, we conducted a rapid survey of the proposed measurement locations in order to ensure that the strength of the received signal would be adequate at all locations. Next, over a span of several days, the operator drove the propagation measurement van to each of the fixed measurement locations that we had selected in advance. At each location, the operator collected simultaneous time series of the received strength of the 220, 850 and 1900 MHz CW signals. The measured data were collected in the form of three successive 120 second sweeps. For the two upper bands, the pair of Anritsu MS2651B spectrum analyzers were used to record three sweeps of 501 samples each, yielding 1503 received signal strength samples at each location. For the 220 MHz band, the Anritsu MS2721A spectrum analyzer was used; it yielded 551 samples per sweep or 1653 samples at each location.

Time-series recordings of received signal strength of 6 minutes in duration as measured at a typical location at a distance of 1.44 km from the transmitting site are shown in Figure 3.2. The upper trace is the 220 MHz received signal; its average received signal strength is -47 dBm and its Ricean K-factor is 24.2 dB. The lower trace is the 1900 MHz received signal; its average received signal strength is -53 dBm and its Ricean K-factor is just 7.4 dB. The K-factor values are very similar to the averages over all locations at each frequency. The greater severity of the signal fading at 1900 MHz compared to 220 MHz is apparent.

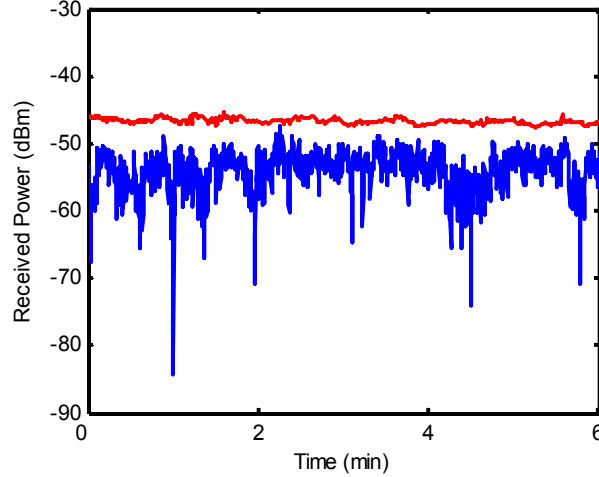


Figure 3.2 Typical time series of received signal strength at 220 MHz (top) and 1900 MHz (bottom) with Ricean K-factors of 24.2 and 7.4 dB, respectively.

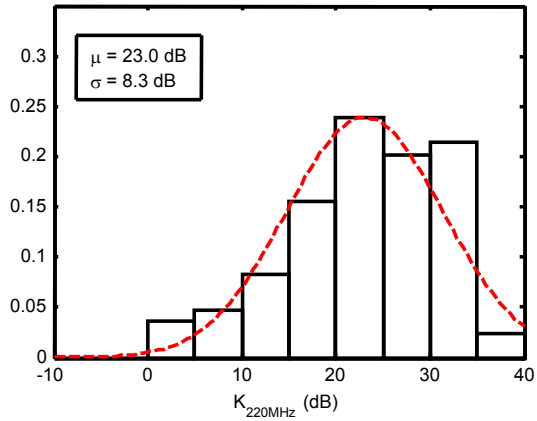
3.4 Results

3.4.1 Distribution of Ricean K-factors

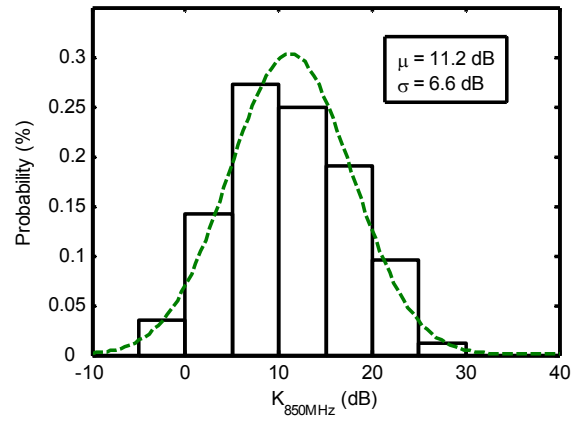
Over the 84 measurement locations and in all three frequency bands, the fading distributions experienced by the received signal are well approximated by Ricean distributions. The Ricean K-factors in each band tend to follow a lognormal distribution (*i.e.*, normal in dB), as suggested by Figure 3.3. The mean values of K are strongly dependent on the frequency band with $\bar{K}_{220} = 23$ dB \gg $\bar{K}_{850} = 11.2$ dB $>$ $\bar{K}_{1900} = 7.7$ dB. Although our results are only based upon three frequencies, we made a preliminary attempt to use regression analysis to determine the relationship between \bar{K} and the carrier frequency. The resulting regression line is shown in Figure 3.4 and is given by

$$\bar{K}(\text{dB}) = -16.6 \log_{10}(f) + 61.5, \quad (3.6)$$

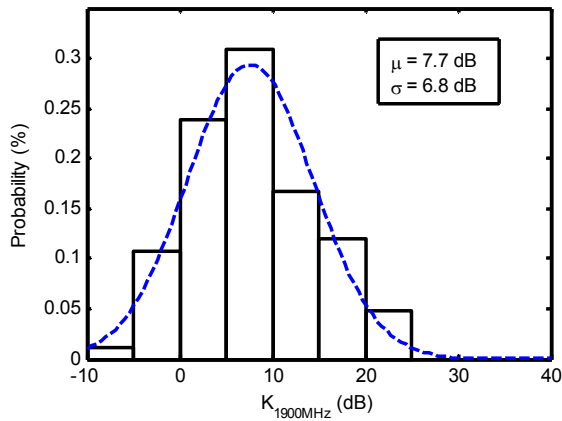
where \bar{K} is expressed in dB and the carrier frequency f is expressed in MHz. The variability of K over all locations at each frequency is remarkably similar and falls between 6.8 and 8.3 dB, a range of less than 1.5 dB. Although these results should be regarded as preliminary because they are based upon only three frequencies, the trend is consistent with the notion that \bar{K} is inversely proportional to $\log_{10}(f)$. It also suggests that the frequency dependence of \bar{K} be investigated further.



(a)



(b)



(c)

Figure 3.3 Distribution of Ricean K-factors observed throughout the test area at (a) 200MHz, (b) 850MHz, and (c) 1900MHz.

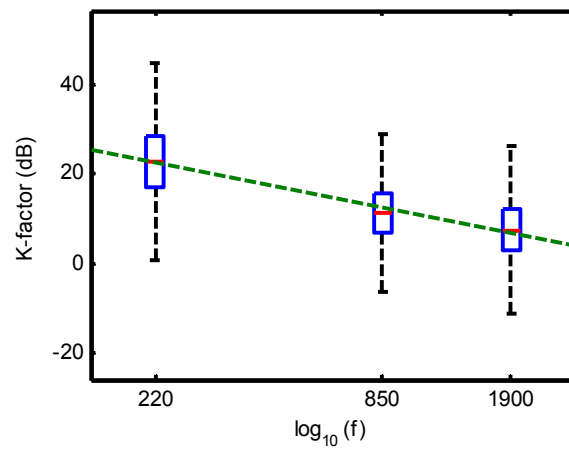


Figure 3.4 Regression analysis of Ricean K-factors vs. carrier frequency in MHz. The distribution of K at 220, 850 and 1900 MHz is indicated by a box plot.

If, as seems likely, the scattered component of the received signal is the result of scattering by windblown trees and foliage, the frequency dependence of the severity of fading can likely be explained by considering the displacement of the moving scatterers in terms of the wavelength of the signal. As wavelength increases, a given displacement of leaves and branches by the wind will lead to a much smaller phase shift of the scattered signal and a much lower probability of deep fades occurring at the receiver. In [53], [54] and [55], the first attempts to formulate physical models capable of predicting and/or simulating fading on fixed wireless channels due to moving vegetation were reported. Development of a more sophisticated physical model that captures the frequency dependence of fading reported here is an obvious next step.

3.4.2 Path Gain and Ricean K-factors vs. Distance

We used (3.2) and (3.4) to estimate the values of G and K , respectively, that describe the set of time series data collected at each location, then plotted the results vs. the distance between the transmitter and the receiver. Path gain and Ricean K-factor both decrease with distance according to a power law relationship as suggested by Figures 3.5(a) and (b). We characterized the distance dependence of G and K by estimating the regression line that best fits the measured data. We also estimated the correlation coefficients ρ between each parameter and distance d and estimated the location variability σ of the parameter, *i.e.*, the variation of the parameter about the regression line. The regression lines for G and K and the corresponding correlation coefficients ρ and location variabilities σ in each frequency band are given by

$$\bar{G}_{220}(\text{dB}) = -33.5 \log_{10} d - 92.3; \quad \rho = -0.59, \sigma = 7.2, \quad (3.7)$$

$$\bar{G}_{850}(\text{dB}) = -37 \log_{10} d - 108.4; \quad \rho = -0.64, \sigma = 6.9, \quad (3.8)$$

$$\bar{G}_{1900}(\text{dB}) = -36 \log_{10} d - 114.7; \quad \rho = -0.58, \sigma = 7.9, \quad (3.9)$$

and

$$\bar{K}_{220}(\text{dB}) = -8.0 \log_{10} d + 25.8; \quad \rho = -0.15, \sigma = 8.3, \quad (3.10)$$

$$\bar{K}_{850}(\text{dB}) = -4.9 \log_{10} d + 12.9; \quad \rho = -0.12, \sigma = 6.5, \quad (3.11)$$

$$\bar{K}_{1900}(\text{dB}) = -8.5 \log_{10} d + 10.5; \quad \rho = -0.19, \sigma = 6.7, \quad (3.12)$$

respectively, where the parameters' subscript indicate the relevant frequency band in MHz and all values of σ are given in dB. For simplicity, subscripts have not been added to either ρ or σ ; it is understood that each instance applies only to the corresponding regression line.

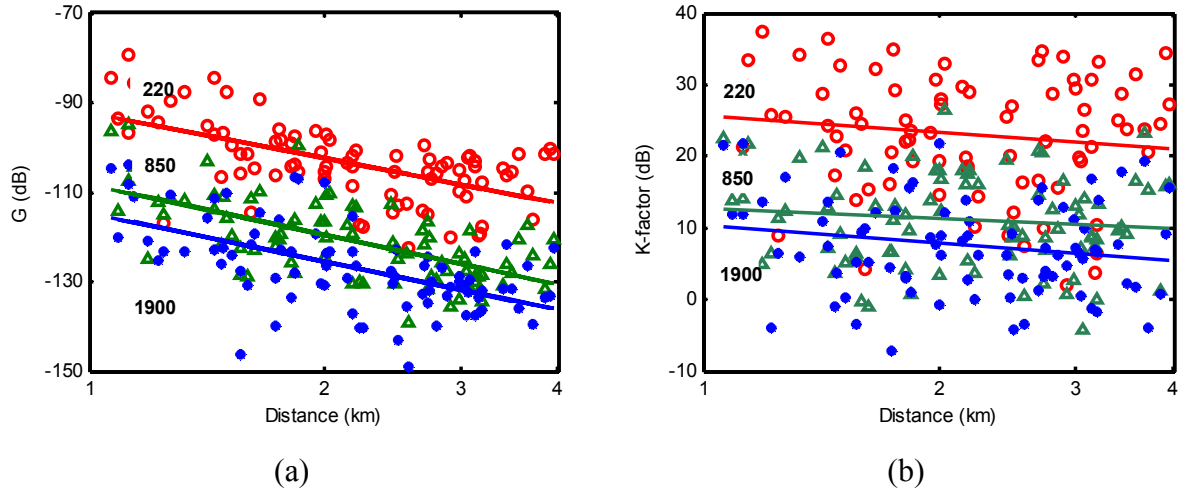


Figure 3. 5 (a) Average path gain G and (b) Ricean K -factors observed at 220 (O), 850 (Δ), and 1900 (\bullet) MHz vs. distance.

Path gain changes with distance and frequency in the general manner predicted by standard models. The distance coefficients in (3.7)-(3.9) are 33.5, 37 and 36, respectively. They are higher than but comparable to the value of 32 that the Okumura-Hata/COST-231 model predicts for a high transmitting site and light-to-moderate foliage with gentle terrain in the coverage area [13]. We also note that the exponent increases slightly as the frequency increases. In general, approximately two-thirds of the differences in path gain (in dB) between frequencies can be attributed to the reduction in the effective area of the receiving antenna as frequency increases. The remaining third can likely be attributed to increased diffraction losses as the frequency increases. For a given distance d , $\bar{K}_{220}(d) \gg \bar{K}_{850}(d) > \bar{K}_{1950}(d)$. Moreover, K falls off with increasing distance, but at a much slower rate than path gain. The location variability of K is comparable to that of path gain.

3.4.3 Fixed and Scattered Path Gain vs. Distance

Our second set of reductions involved estimating the fixed path gain G_f and the scattered path gain G_s associated with the set of time series data collected at each location. These parameters are given by the numerator and denominator of (3.4), respectively, so provide insight into the behavior of K . Because fixed path gain tends to be determined by the

configuration of obstacles along the direct path between the base and remote terminal while scattered path gain is the result of scattering over a broad range of angles about the remote terminal, we anticipated that G_f would roll off with distance more quickly and experience greater location variability than G_s . However, few previous studies have either verified these trends or quantified them. We plotted the results vs. the distance between the transmitter and receiver; the results are presented in Figures 3.6(a) and (b).

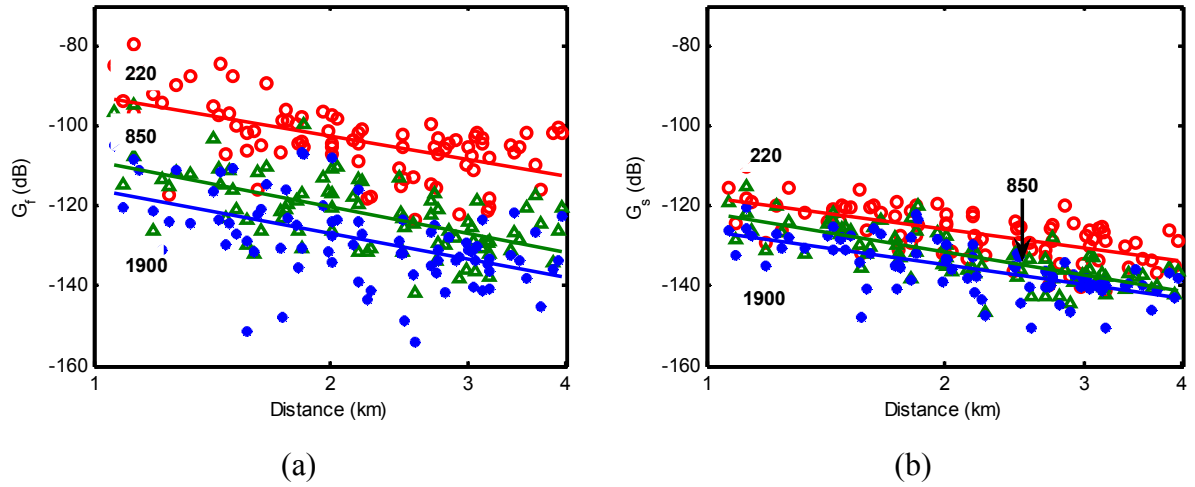


Figure 3.6 (a) Fixed path gain G_f and (b) scattered path gain G_s , observed at 220 (O), 850 (Δ), and 1900 (\bullet) MHz vs. distance.

Fixed and scattered path gain both decrease with distance according to a power law relationship. The regression lines for G_f and G_s and the corresponding correlation coefficients and location variabilities in each frequency band are given by

$$\bar{G}_{f_{220}}(dB) = -33.8 \log_{10} d - 92.3; \quad \rho = -0.58, \sigma = 7.4, \quad (3.13)$$

$$\bar{G}_{f_{850}}(dB) = -37.6 \log_{10} d - 108.9; \quad \rho = -0.61, \sigma = 7.5, \quad (3.14)$$

$$\bar{G}_{f_{1900}}(dB) = -36.9 \log_{10} d - 115.7; \quad \rho = -0.53, \sigma = 9.1, \quad (3.15)$$

and

$$\bar{G}_{s_{220}}(dB) = -25.8 \log_{10} d - 118.1; \quad \rho = -0.65, \sigma = 4.7, \quad (3.16)$$

$$\bar{G}_{s_{850}}(dB) = -32.7 \log_{10} d - 121.7; \quad \rho = -0.77, \sigma = 4.2, \quad (3.17)$$

$$\bar{G}_{s_{1900}}(dB) = -28.4 \log_{10} d - 126.2; \quad \rho = -0.67, \sigma = 4.9, \quad (3.18)$$

respectively. Once again, the subscripts indicate the relevant frequency in MHz and all values of σ are given in dB. Also, subscripts have not been added to either ρ or σ ; it is understood that the values given with the expression for each regression line apply to that regression line.

Three trends are immediately apparent: 1) At all three frequencies, the fixed path gain falls off with distance more quickly than does the scattered path gain. This, of course, is what causes K-factor to decrease as distance increases. 2) At all three frequencies, the location variability of scattered path gain is between 2.5 and 4 dB less than the location variability of the corresponding fixed path gain. This is consistent with our physical understanding of the nature of fixed and scattered path gains, as summarized earlier in this section. 3) At a given distance, the mean scattered path gain at each frequency is only a few dB different from those at other frequencies. The differences between the corresponding fixed path gains are far greater.

If one normalizes the path gains by removing the frequency-squared dependence of the free space path loss component, two further trends are apparent: 1) the normalized fixed path gain at lower frequencies is greater than at higher frequencies, likely because diffraction losses are less and 2) the normalized scattered path gain at lower frequencies is less than at higher frequencies, likely because the obstructions and scatterers in the environment are smaller in terms of wavelength and do not diffract and scatter wireless signals as effectively.

3.4.4 Excess Path Gain and Ricean K-factor as a Function of Average Wind Speed

Our third set of data reductions involved determining how path gain and the Ricean K-factor observed at each location are affected by the time-averaged wind speed v in km/h that we observed in the vicinity of the transmitting site. In order to remove the distance dependence from path gain, we calculated the excess path gain ΔG (or the difference in dB) between the path gain G measured at a given location and the mean value \bar{G} observed at that distance. Because Ricean K-factor depends only weakly on distance, and to be consistent with the approach taken by others, we ignored that distance dependence of K and simply compared K

to wind speed. The results are presented in Figures 3.7(a) and (b) while the distribution of average wind speeds that we observed over all measurements is presented in Figure 3.8.

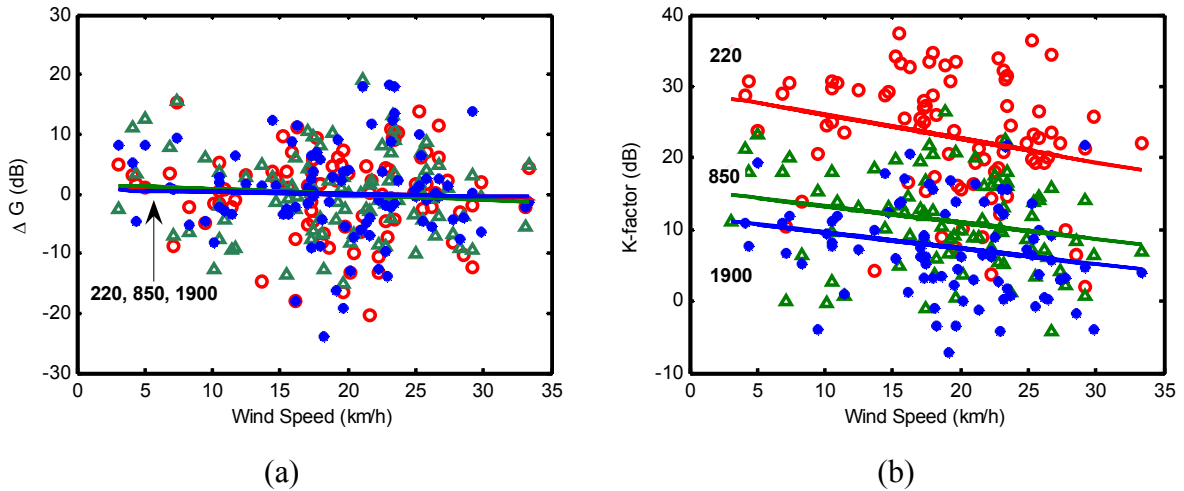


Figure 3.7 (a) Excess path gain and (b) Ricean K-factors observed at 220 (O), 850 (Δ), and 1900 (\bullet) MHz vs. averaged wind speed.

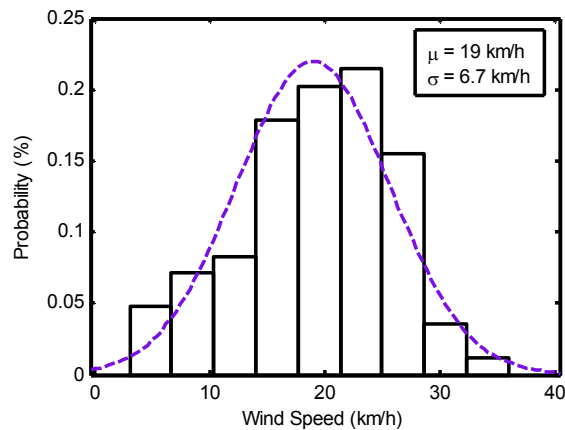


Figure 3.8 The average wind speed distribution observed at the base station during data collection.

We estimated the regression line that best fits the measured data, the correlation coefficient between each parameter and the average wind speed, and the location variability of the parameter, *i.e.*, the variation of the parameter about the regression line at a given average wind speed. The regression lines for ΔG and K and the corresponding correlation coefficients and location variabilities in each frequency band are given by

$$\Delta \bar{G}_{220}(dB) = -0.037v_w + 0.69; \quad \rho = -0.034, \sigma = 7.2, \quad (3.19)$$

$$\Delta \bar{G}_{850}(dB) = -0.058v_w + 1.11; \quad \rho = -0.057, \sigma = 6.9, \quad (3.20)$$

$$\Delta \bar{G}_{1900}(dB) = 0.001v_w - 0.02; \quad \rho = 0.001, \sigma = 7.9, \quad (3.21)$$

and

$$\bar{K}_{220}(dB) = -0.33v_w + 29.4; \quad \rho = -0.26, \sigma = 8.3, \quad (3.22)$$

$$\bar{K}_{850}(dB) = -0.23v_w + 15.5; \quad \rho = -0.23, \sigma = 6.6, \quad (3.23)$$

$$\bar{K}_{1900}(dB) = -0.22v_w + 11.9; \quad \rho = -0.22, \sigma = 6.8, \quad (3.24)$$

respectively, where v_w is expressed in km/h.

As expected, there is no correlation between the excess path gain and average wind speed. Both the moderate negative correlations between the Ricean K-factor and average wind speed and the standard deviations at all three frequencies are comparable to each other. The main differences between (3.22)-(3.24) are the intercepts of the regression lines with the K axis, which decrease as the carrier frequency increases.

3.4.5 Excess Fixed Path Gain and Excess Scatter Path Gain as a Function of Average Wind Speed

Our fourth set of data reductions involved determining how the fixed and scattered path gains are affected by the average wind speed. As in the previous section, we eliminated the distance dependence of path gain by taking the excess value of each parameter or the difference (in dB) between the parameter measured at a given location and the mean value observed at that distance. The results are presented in Figures 3.9(a) and (b).

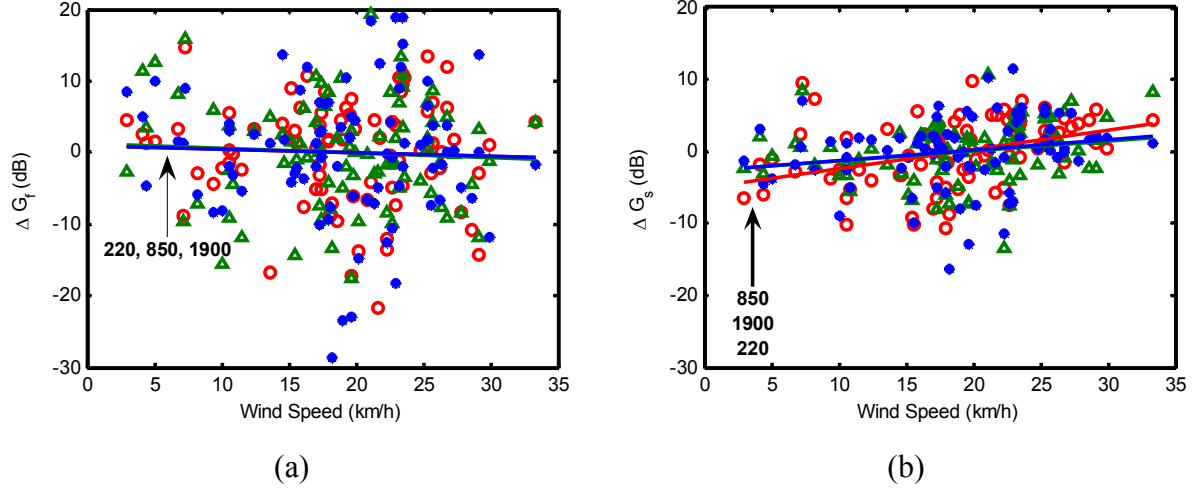


Figure 3.9 (a) Excess fixed path gain and (b) excess scattered path gain observed at 220 (O), 850 (Δ), and 1900 (●) MHz vs. average wind speed.

We estimated the regression line that best fits the measured data, the correlation coefficient between each parameter and the average wind speed, v_w , and the location variability of the parameter, *i.e.*, the variation of the parameter about the regression line at a given average wind speed. The regression lines for ΔG_f and ΔG_s and the corresponding correlation coefficients and location variabilities in each frequency band are given by

$$\Delta \bar{G}_{f_220}(dB) = -0.044v_w + 0.84; \quad \rho = -0.04, \sigma = 7.4 \quad (3.25)$$

$$\Delta \bar{G}_{f_850}(dB) = -0.072v_w + 1.37; \quad \rho = -0.064, \sigma = 7.5 \quad (3.26)$$

$$\Delta \bar{G}_{f_1900}(dB) = -0.048v_w + 0.9; \quad \rho = -0.035, \sigma = 9.1 \quad (3.27)$$

and

$$\Delta \bar{G}_{s_220}(dB) = 0.26v_w - 5.0; \quad \rho = 0.37, \sigma = 4.7, \quad (3.28)$$

$$\Delta \bar{G}_{s_850}(dB) = 0.14v_w - 2.6; \quad \rho = 0.22, \sigma = 4.2, \quad (3.29)$$

$$\Delta \bar{G}_{s_1900}(dB) = 0.15v_w - 2.9; \quad \rho = 0.21, \sigma = 4.9, \quad (3.30)$$

respectively.

As expected, there is no correlation between the excess fixed path gain and average wind speed. In contrast, there is a clear relationship between scattered path gain and wind speed. The moderate positive correlations between the excess scattered path gain and average wind speed at all three frequencies are comparable to each other, as are the standard deviations. The main differences are the intercepts of the regression line with the ΔG_s axis, which generally decreases as the carrier frequency increases.

3.4.6 Joint Dependency of the Excess Path Gain and Ricean K-factor

At a given location, we observed a strong correlation between the excess path gain ΔG and the Ricean K-factor. In order to remove distance effects, we replaced K by the excess Rician K-factor ΔK , i.e., the difference in dB between the Rician K-factor observed at a given location and $\bar{K}(d)$ the mean value at that distance which is given by (3.10)-(3.12) for the three frequency bands that we considered. The results are presented in Figure 3.10(a), (b), and (c). The corresponding regression lines are given by

$$\Delta \bar{K}_{220}(dB) = 0.94 \Delta G_{220} + 23.1; \quad \rho = 0.81, \sigma = 4.9, \quad (3.31)$$

$$\Delta \bar{K}_{850}(dB) = 0.75 \Delta G_{850} + 11.23; \quad \rho = 0.78, \sigma = 4.1, \quad (3.32)$$

$$\Delta \bar{K}_{1900}(dB) = 0.68 \Delta G_{1900} + 7.6; \quad \rho = 0.80, \sigma = 4.2, \quad (3.33)$$

Because the dependence of K on distance is so much weaker than its dependence on excess path gain, the correlations given in (3.31)-(3.33) are virtually identical to those that we observed between ΔG and K . This correlation between ΔG and ΔK forms the basis for the simulation model that we present in the next section.

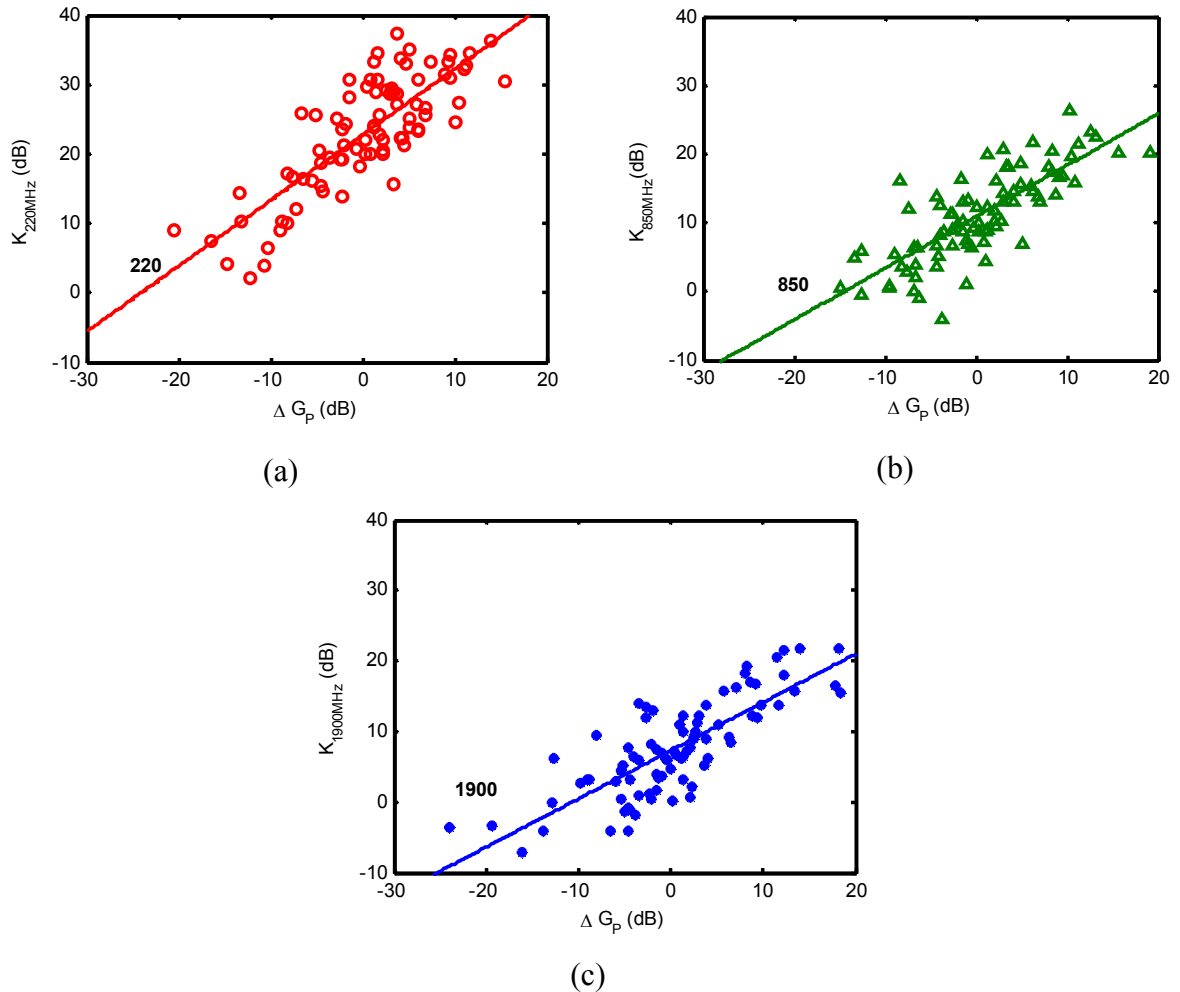


Figure 3.10 Scatter plots of Ricean K-factor vs. excess path loss at a given distance at (a) 220 (O), (b) 850 (Δ), and (c) 1900 (\bullet) MHz.

3.5 A Simulation Model

In simulations of fixed wireless systems, it may be necessary to generate values of G and K that a link might experience at a particular frequency and distance. Although we do not have any information concerning the correlation between the values of G and K in either time or space, we can easily generate values that have the same *first order* statistics as our measured data. In a particular frequency band, we consider G and K as the sum of: 1) the mean value \bar{G} and \bar{K} at a particular distance d and 2) random components ΔG and ΔK which have zero

mean. If, as our results suggest, we can assume that ΔG and ΔK are both normally distributed when expressed in dB, their joint distributions are completely described by their mean values, standard deviations and mutual correlation coefficient. Thus, at a given distance and in a specific frequency band, $G(d)$ and $K(d)$ can be generated by

$$\begin{aligned} G(d) &= \bar{G}(d) + \Delta G \\ &= \bar{G}(d) + \sigma_G U_1 \end{aligned} \quad (3.34)$$

and

$$\begin{aligned} K(d) &= \bar{K}(d) + \Delta K \\ &= \bar{K}(d) + \rho \sigma_K U_1 + \sqrt{1 - \rho^2} \sigma_K U_2 \end{aligned} \quad (3.35)$$

where σ_G is the σ given in (3.7)-(3.9), σ_K is the σ given in (3.10)-(3.12), ρ is given in (3.31)-(3.33), and U_1 and U_2 are uncorrelated Gaussian random variables with zero mean and unit variance.

3.6 Conclusions

To the best of our knowledge, this is the first study to compare path gain and signal fading on fixed NLOS links in suburban macrocell environments over the frequency range 220 MHz to 2 GHz. Our most significant finding is that the depth of signal fading drops off rapidly as frequency decreases (or as wavelength increases). A link that experiences severe fading at 1.9 GHz is often relatively unaffected at 220 MHz. An obvious next step for future researchers will be to develop a more sophisticated physical model that is consistent with the multiband measurement data presented here.

The first-order statistical models that we have presented here capture the essential aspects of the manner in which fixed wireless channels between 200 MHz and 2 GHz fade in a typical suburban macrocell environment. Development of models applicable to a broad range of environments would require additional measurement data: 1) from other sites, 2) from transmitters at different heights and 3) at additional frequencies within the range of interest. Such models will provide a basis for predicting the coverage and outage probabilities experienced by point-to-multipoint fixed wireless networks deployed in suburban macrocell environments and for assessing the suitability of a particular frequency band for use in a given application. The results presented here represent the first step in achieving this goal.

Chapter 4

Effect of Terminal Height on Location Variability of Fixed Wireless Channels at 1.9 GHz in Suburban Macrocell Environments

4.1 Introduction

In macrocell environments, the base station antenna is located well above the local rooftop or treetop level and the remote terminal antenna is mounted below the local rooftop or treetop level. Because the direct line-of-sight is generally blocked, the path loss experienced by such links tends to increase more quickly with distance than it would under free space conditions. Varying degrees of obstruction by natural and man-made obstacles along the propagation path give rise to variations in the path loss at a given distance that are referred to as shadow fading. As the intensity of shadow fading increases, it becomes more likely that the received signal at a given distance will drop below the receiver threshold and the gaps in coverage experienced by remote terminals at a given distance will become larger and more common.

Previous work has shown that location variability is a lognormal random variable about the mean path loss at a given distance and has revealed how it varies with carrier frequency, clutter density and base station height [15],[56],[57],[58]. The tendencies for location variability to increase with carrier frequency and to increase with building density and building height distribution are well known. Recent path loss models also show how location variability is affected by changes in the height of the base station. Virtually all previous work concerning location variability has focused on remote terminals with heights of between 1.5 and 2 metres, which is sufficient for planning and assessing the vast majority of land mobile and portable communications systems currently deployed in macrocell environments.

In the near future, wireless relays and terminals will be mounted on lamp poles and distribution poles at heights of between 5 and 7 metres above ground level in order to support emerging applications that employ relay-based architectures such as Distribution Automation, Intelligent Transportation Systems and advanced cellular radio systems such as WiMAX and Long Term Evolution (LTE). Using location variability estimates based upon measurements collected at far lower terminal heights could result in inaccurate coverage predictions and degraded system reliability. While intuition might suggest that shadow fading

will decrease with increasing terminal height, the literature offers few, if any, insights or confirmatory evidence.

Here, we take the first steps to resolving this issue by comparing the location variability that we observed at different terminal heights in both simulated and measured path loss data collected in a typical suburban macrocell environment. The remainder of this chapter is organized as follows: In Section 4.2, we describe the test site. In Section 4.3, we describe the setup used to generate the simulated path loss data. In Section 4.4, we describe the setup used to collect the measured path loss data. In Section 4.5, we compare the location variability observed as a function of terminal height in both the simulated and measured data. In Section 4.6, we draw conclusions and offer recommendations for further work.

4.2 The Test Site

Our test site consisted of suburban neighborhoods with generally flat terrain, light to moderate foliage and one-and two-storey houses between 300 m and 3 km from BC Hydro's Edmonds facility in Burnaby, BC. The building density at the site is 100 structures per square kilometer with an average separation between structures of 20 metres. With the assistance of photogrammetry specialists at BC Hydro, we acquired the height of buildings and trees at 84 randomly selected locations within the site. The mean clutter height was 10m. The clutter height distribution followed a normal distribution.

4.3 The Simulator

We used Wireless InSite, a powerful ray-tracing-based wave propagation simulator, to predict the effects of obstruction by buildings and trees on the wireless propagation within a simulated test site in which the building density and heights have the same statistical distribution as those within the actual test site. A portion of the simulated test site is shown in Fig. 4.1.

Within the Wireless InSite simulator, we set the frequency of operation to 1900 MHz and the signal bandwidth to 1 MHz. The omnidirectional transmitting antenna was positioned at the middle of the test site at a height of 80 m. At each of thirty randomly selected receiver locations, we determined the path loss experienced by receivers at seven different heights: 2, 7, 9, 11, 13, and 15 m. The outputs of the simulation were 30 text files whose contents were

imported into MATLAB for further analysis. The distribution of the clutter height used during simulation is how in figure 4.1 below

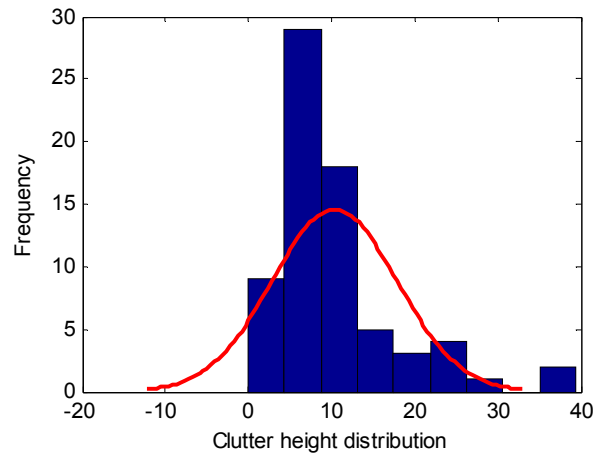


Figure 4.1– Distribution of clutter height.

4.4 The Measurement Setup

We used the same base station, channel sounder, measurement setup, and test area that was described in Chapter 3. We mounted a 1.9 GHz antenna on the roof of the van for measurements at a terminal height of 2 m. We mounted a second 1.9 GHz antenna atop a 6-m telescoping mast that we installed on the rear bumper of the van in order to permit measurements to be collected at terminal heights of 5 and 7 m.

We collected measurement data at 80 fixed locations that were situated within an annulus between 300 m and 3 km from the transmitter site. At each location, we adjusted the mast to a height of 5 m and recorded the time series of the received signal strengths at 2 m and 5 m. Next, we adjusted the mast to record time series of the received signal strengths at 7 m before moving to the next location. The measured data were collected in the form of three successive 120-second sweeps; each sweep yielded 501 samples for a total of 1503 received signal strength samples at each location. These were linearly averaged to yield the average received signal strength, and then further processed to yield the average path gain at each location and at each terminal height.

4.5 Results

We processed our simulated and measured data to find the regression line that best fit path gain vs. distance at each terminal height. We then extracted the shadow-fading component or *shadow loss* and estimated the standard deviation of the lognormal distribution that best fit the data.

4.5.1 Simulation Results

The simulated path gain and regression line vs. distance for a terminal height of 7 m is shown in Figure 4.2. The shadow fading component vs. distance for a terminal height of 7 m is shown in Figure 4.3. Similar results were extracted for the other six terminal heights.

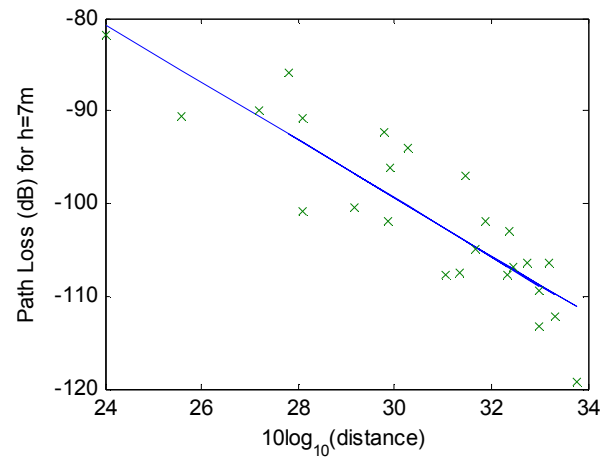


Figure 4.2 - Simulated path gain vs. distance. Solid line shows the mean path gain (regression line)

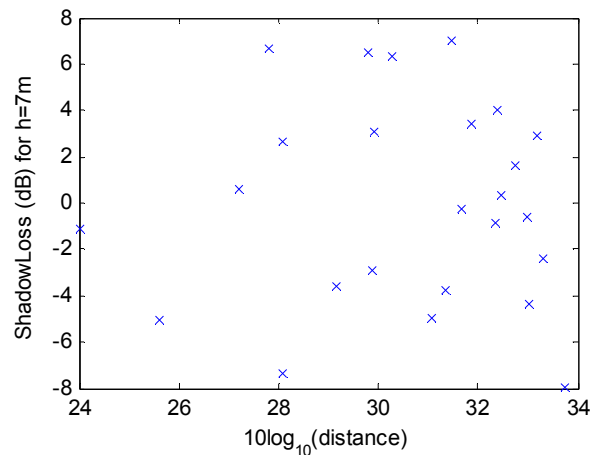


Figure 4.3 - Shadow loss in dB for different distances from transmitter antenna at height h=7m.

The next step was to generate the distribution of shadow loss by applying the best normal distribution fit to the data. Figure 4.4 shows the shadow loss distribution at terminal heights of 2, 5 and 7 m. The corresponding estimates of the standard deviation at these terminal heights are 3.4, 3.9 and 4.9 dB, respectively.

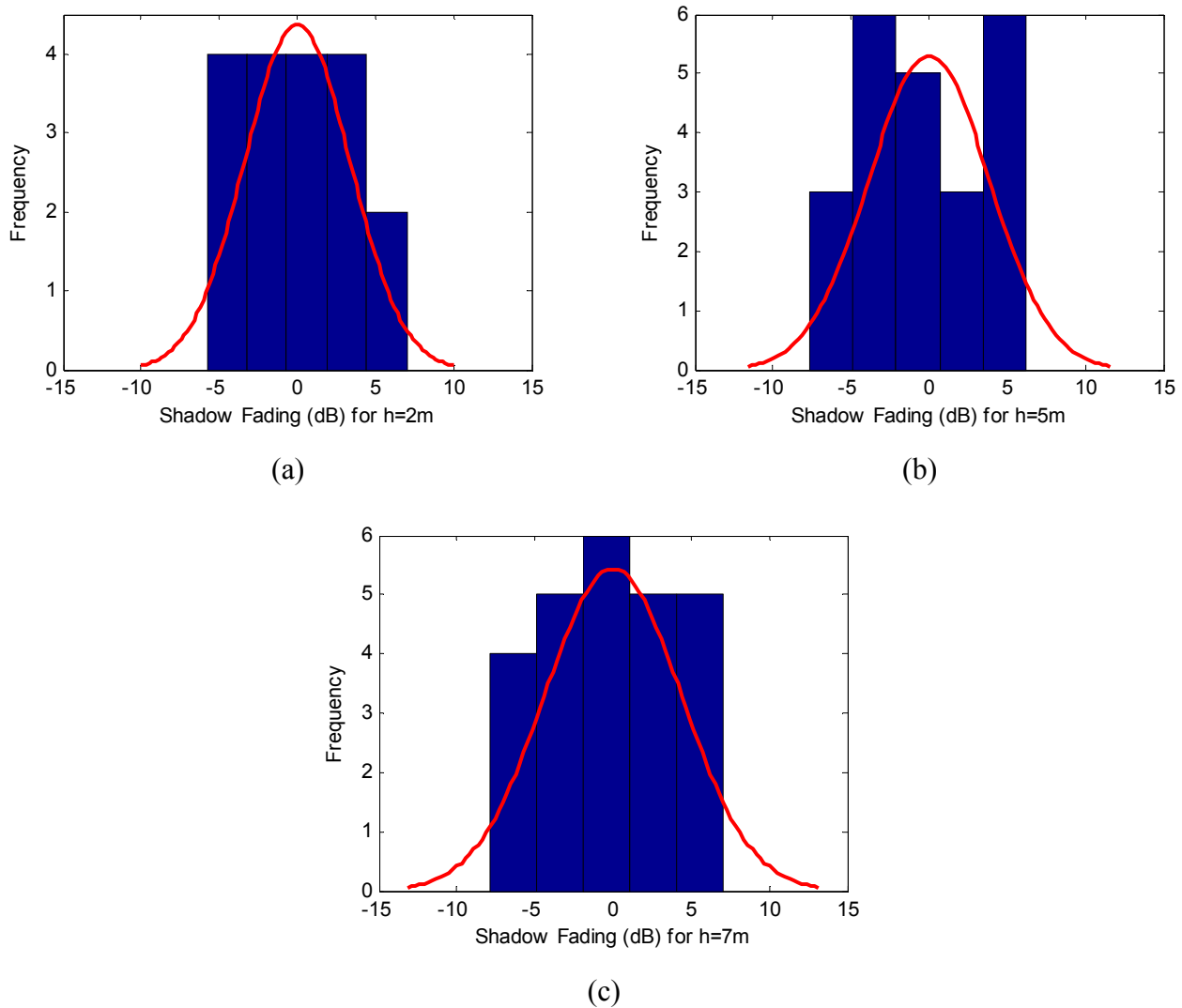


Figure 4.4 - Shadow loss in dB for receiving antennas at heights of (a) 2m, (b) 5m, and (c) 7 m.

We plotted the location variability for the seven different heights to better understand the effect of height on location variability. The result is shown in Figure 4.5. The simulation shows that location variability increases with terminal height until it matches the mean clutter

distribution height. As terminal height increases further, location variability slowly decreases.

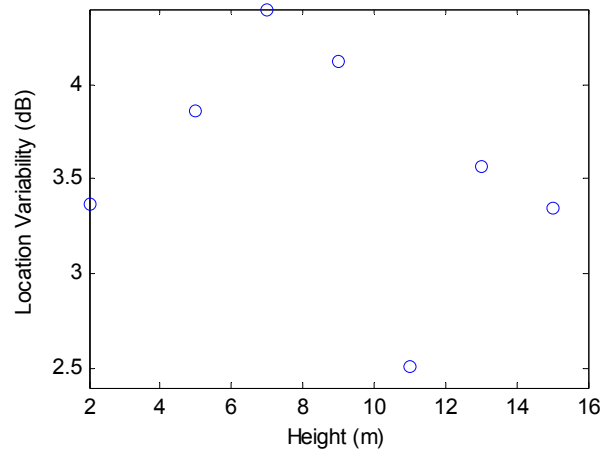


Figure 4.5 – Location variability with different heights of receiving antenna

4.5.2 Measurement Results

4.5.2.1 Path Gain vs. Distance

We characterized the distance dependence of path gain at receiving antenna heights of 2, 5 and 7 m by estimating the regression line that best fits the measured data in a least squares sense. We also estimated the value of Pearson's correlation coefficient ρ between each parameter and distance d and estimated the location variability σ of the parameter, i.e., the standard deviation of the residuals. Pearson's correlation coefficient provides a useful indication of the goodness of fit of the line and our confidence in the estimates of the slope and intercept of the regression line. The results are shown in Figure 4.6 and 4.7. The measured best path gain values occurred at the heights of 5 and 7m. However during the worst measured path gain conditions, the path gains at 5m and 7m were as bad as at the lower height of 2m. Also the path gains at greater heights display more variability than at 2 m.

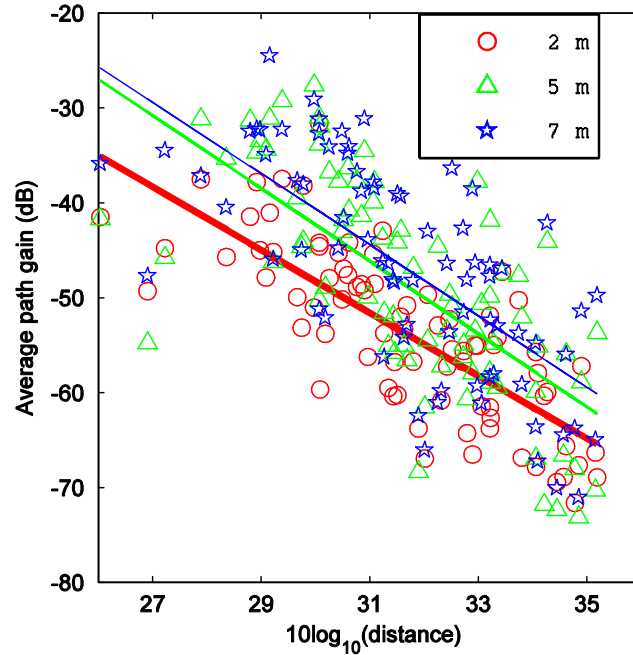


Figure 4.6 – Average path gain observed at terminal heights of 2, 5 and 7 m vs. distance

The regression lines for average path gain and the corresponding correlation coefficients and location variability at each height are given by:

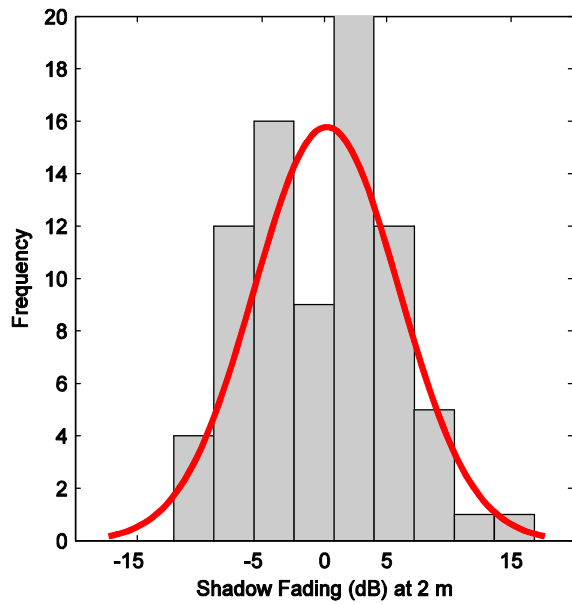
$$\bar{G}_2(\text{dB}) = -33 \log_{10} d + 51; \quad \rho = -0.76, \quad \sigma = 5.7, \quad (4.1)$$

$$\bar{G}_5(\text{dB}) = -38 \log_{10} d + 72.5; \quad \rho = -0.69, \quad \sigma = 8.1, \quad (4.2)$$

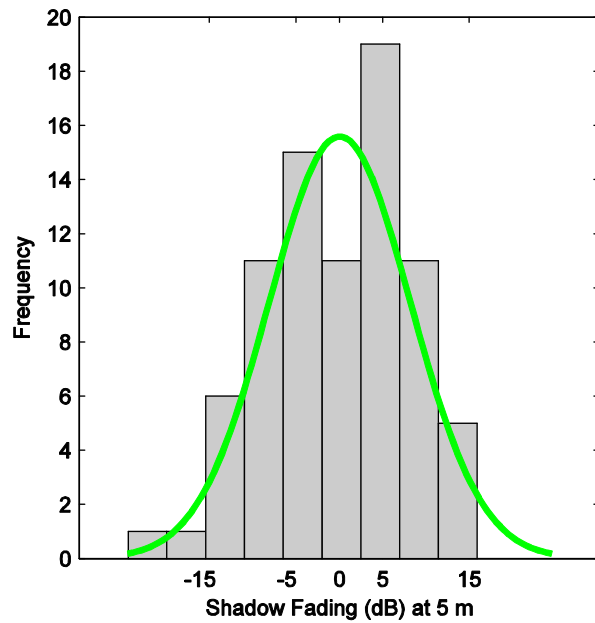
$$\bar{G}_7(\text{dB}) = -37 \log_{10} d + 71.7; \quad \rho = -0.69, \quad \sigma = 8.0, \quad (4.3)$$

respectively, where each parameter's subscript indicates the relevant terminal height in metres and all values of ρ and σ are given in dB. For simplicity, subscripts have not been added to either ρ or σ ; it is understood that each instance applies only to the corresponding regression line.

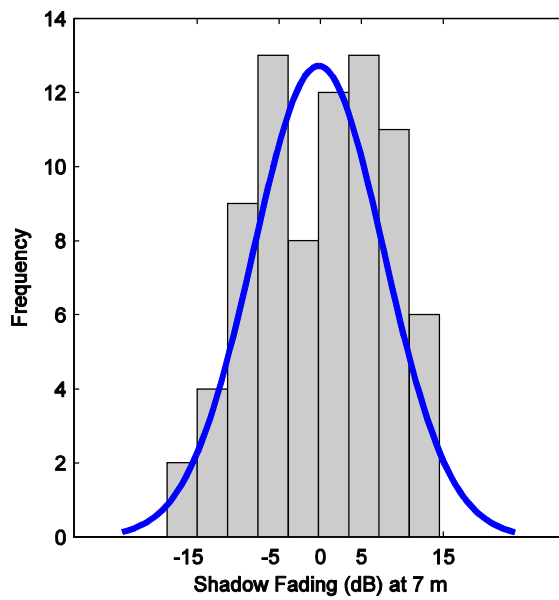
At each height, path gain decreases with distance according to a power law relationship as predicted by standard models. The distance coefficient in (4.1)-(4.3) are 33, 38 and 37 respectively. They are higher than but comparable to the value of 32 that the Okumura-Hata/COST-231 model predicts for a high transmitting site and a light-to-moderate foliage with gentle terrain in the coverage area [13],[14]. They are also consistent with the values of 34.5 and 36 that the AT&T model predicts for gentle terrain with light and moderate foliage respectively [15].



(a)



(b)



(c)

Figure 4.7- Shadow fading distribution observed throughout the test area at terminal heights of (a) 2 m, (b) 5 m, and (c) 7 m where $\sigma = 5.7, 8.1$ and 8.0 dB, respectively.

4.6 Conclusions

The simulated and measured results presented here both suggest that while mean path gain always tends to increase as terminal height increases, location variability reaches its maximum value when the terminal height approaches the mean building height. As the terminal height rises or falls past this value, location variability decreases. For this reason, raising a wireless relay or terminal from pedestrian to pole-top level may not increase the area coverage of the base-station-to-pole-top link as much as the increase in mean path gain might otherwise suggest. Further work based upon other environments is required to fully reveal the empirical relationship between the building height distribution in a given neighbourhood and the manner in which location variability of path loss varies with relay or terminal height.

Chapter 5

Conclusion and Recommendations

5.1 Conclusions

Because private wireless networks are generally less expensive, easier to deploy and more resilient than alternatives such as fibre-optic, power line carrier (PLC) or common carrier networks, they have attracted considerable interest from designers of Distribution Automation (DA) networks. However, designers of such wireless networks must account for: 1) the manner in which the useful range of the links between wireless devices impacts the formation of wireless DA networks, 2) the depth of fading varies across the range of frequencies available to power utilities for use in such networks, and 3) the degree of shadow fading varies as the height of wireless devices used in such networks rise from pedestrian to pole-top level.

The manner in which the capacitor banks, reclosers and voltage regulators in BC Hydro's distribution grid and the BC Hydro substations and microwave repeater sites that could host macrocell base stations are geographically dispersed throughout the province affects the ease with which these assets can be formed into either conventional base-station-to-pole-top fixed wireless macrocell networks or pole-top-to-pole-top fixed wireless mesh networks. Only three-quarters of these assets are located within 10 km of BC Hydro's existing substations or microwave repeater sites. Thus, additional base station sites will need to be acquired if conventional WiMAX-based base-station-to-pole-top fixed wireless macrocell networks are used to implement Distribution Automation. However, almost none of the distribution assets are located within 1 km of another. Thus, using a ZigBee-based mesh network to implement DA is problematic. While private wireless networks present many advantages, it seems likely that they must be supplemented by other techniques if DA is to reach the entire province.

Regulators have allocated several frequency bands between 200 MHz and 2 GHz for use by electrical power utilities in Distribution Automation networks. Although the bandwidth available at lower frequencies is considerably less than what is available at higher frequencies, the depth of fading experienced on fixed wireless macrocell channels drops off rapidly as frequency decreases (or as wavelength increases). A link that experiences severe

fading at 2 GHz is often relatively unaffected at 200 MHz. Thus, selection of a particular frequency band for a particular DA application represents a tradeoff between link quality and available bandwidth and must be carefully considered.

As the degree of shadow fading experienced on fixed wireless macrocell channels increases, the number of holes and gaps in the coverage of a base station increases, particularly at greater ranges. While it is often assumed that the degree of shadow fading will decrease monotonically as the height of the remote terminal increases, we have presented convincing evidence that the degree of shadow fading actually reaches its maximum value when the remote terminal is at or near the mean height of the buildings and other obstructions in the local environment. Thus, raising the terminal height from pedestrian to pole-top level may not improve the system link budget as much as the increase in mean path gain might otherwise suggest.

5.2 Recommendation for Future Work

The results presented in this thesis represent a first effort to characterize fixed wireless channels in scenarios of the type likely to be encountered in Distribution Automation networks. The principal limitation of our work is that all data was collected at a single site. An obvious next step is to collect data at other sites in order to yield a richer base of data. We further suggest that future efforts to extend our understanding of fixed wireless channels should include:

- 1. Development of base station site selection algorithms that will help designers choose the most appropriate combination of base station sites to cover a given set of distribution assets.*

While base station site selection algorithms have previously been developed for cellular networks, DA assets are distributed over a vast range and are relatively sparse. A site selection algorithm expressly designed for planning macrocell-based DA networks might be more effective than those currently available.

- 2. Development of a measurement-based site-general path loss model applicable to pole-top-to-pole-top links in wireless mesh networks over distances of between 200 and 1200 metres.*

In such cases, the direct line of sight between wireless devices will generally be blocked and path loss will generally be higher than in the free space or line-of-sight cases. Such models should account for both mean and excess path loss observed on a given link and

the correlation between excess path loss observed on links to different nodes. Initial efforts should focus on development of measurement-based models.

3. *Further study the manner in which the degree of shadow fading experienced on fixed wireless macrocell channels changes with the height of the remote terminal.*

The results presented in this thesis only apply to a particular, albeit typical, suburban neighbourhood. Further data should be collected in a variety of neighbourhoods in order to better understand the relationship between building height distribution and the manner in which the degree of shadow fading experienced on fixed wireless macrocell channels changes with the height of the remote terminal.

References

- [1] North American Electric Reliability Corporation, [Online]. [Available]: www.nerc.com
- [2] United States Congress. (2007, December). Energy Independence and Security Act. Washington,DC.[Online]. Available: http://energy.senate.gov/public/_files/getdoc1.pdf
- [3] European Commission. (2006). European Smart Grids Technology Platform. Brussels, Belgium. [Online]. Available: http://ec.europa.eu/research/energy/smartgrids.en_pdf
- [4] K. Ogawa. (2009, Dec). Japan's initiatives on smart grid – A proposal of “Nature Grid”. Brussels, Belgium. [Online]. Available: http://documents.eu-japan.eu/seminars/Europe/Other/smart_grid/report.pdf
- [5] BC Hydro. (2009, Dec). Smart Metering & Infrastructure Program Business case. Victoria,BC.[Online].Available:<http://www.BCHydro.com/etc/medialib/internet/documents/smi>
- [6] National Institute of Standards and Technology. (2010, Jan.). NIST Framework and Roadmap for Smart Grid Interoperability Standards. [Online]. Available: http://www.nist.gov/public_affairs
- [7] International Electrotechnical commission, SMB Smart Grid Strategic Group (SG3). (2010, Jun). IEC Smart Grid Standardization Roadmap. [Online]. Available: http://www.iec.ch/smartgrid/downloads/sg3_roadmap.pdf
- [8] OpenSmartGrid. (2010, Jul). Smart Grid Networks System Requirements Specification. [Online]. Available: <http://osgu.ucaiug.org>
- [9] IEEE P2030. (2010, Oct). Draft Guide for Smart Grid Interoperability of Energy Technology and Information Technology Operation with the Electric Power System (EPS), and End-Use Applications and Loads. [Online]. Available: <http://smartgrid.ieee.org/publications-smart-grid-publications>
- [10] Industry Canada, “Technical Requirements for Fixed Radio Systems Operating in the Bands 1700-1710 and 1780-1850 MHz”, SRSP-101.7, Jun. 2009
- [11] Industry Canada, “Technical Requirements for Land Mobile and Fixed Radio Systems Operating in the Bands 220-222 MHz”, SRSP-512, Apr. 2006
- [12] Industry Canada, “Policy for the Use of 700 MHz Systems for Public Safety Applications and other Limited Use of Broadcasting Spectrum”, Radio Systems Policy RP-006, Jun. 2006
- [13] M. Hata, “Empirical formula for propagation loss in land mobile radio services,” *IEEE Trans. Veh. Technol.*, vol. 29, no. 3, pp. 317-325, Aug. 1980
- [14] E. Damosa, Ed., “Digital Mobile Radio Toward Future Generation Systems - Final Report,” COST 231 Final Report, 1996.
- [15] V. Erceg, L. J. Greenstein, S. Y. Tjandra, S.R. Parkoff, A. Gupta, B. Kulic, A. A. Julius, and R. Bianchi, “An empirically based path loss model for wireless channels in suburban environments,” *IEEE J. Sel. Areas Commun.*, vol. 17, no. 7, pp. 1205-1211, July 1999.

- [16] United Telecom Council. (2007, Nov). Smart Grid Applications: A Guide to Automation Applications and Vendors. [Online]. Available: <http://www.utc.org>
- [17] United Telecom Council. (2008, Aug). Smart Grids: Building a Strategic Technology Roadmap. [Online]. Available: <http://www.utc.org>
- [18] United Telecom Council. (2010, Sept). A Study of Utility Communications Needs: key factors that impact utility communications networks. [Online]. Available: <http://www.utc.org>
- [19] C. Su and J. Teng, "Economic Evaluation of a Distribution Automation Project," *IEEE Trans. Ind. Appl.*, vol. 43, no.6, pp. 1417-1425, Nov. 2007
- [20] G. Simard and D. Chartrand, "Hydro-Quebec's economic and technical approach to justify its distribution automation program," in Proc. *IEEE PES'07*, 24-28 Jun. 2007, pp. 1-5
- [21] K. Myongsoo and J. Metzner, "A Key Exchange Method for Intelligent Electronic Devices in Distribution Automation," *IEEE Trans. Power Del*, vol.25, no.3, pp. 1458-1464, Jul. 2010
- [22] F. Zavoda, "The key role of Intelligent Electronic Devices (IED) in Advanced Distribution Automation (ADA)", presented at the 2nd Chinese Int. Conf. Electrical Distribution, China, Nov. 2007
- [23] D. Ross, J. Patton, A. Cohen, and M. Carson, "New Methods for Evaluating Distribution Automation and control (DAC) Systems Benefits", *IEEE Trans. Power Apparatus and Systems*, vol. PAS-100, issue 6, pp.2978-2986, Jun. 1981
- [24] W.E Blair and V.T Rhyne, "Communication Systems for Distribution Automation and Load Management. Results of EPRI/DOE Research", *IEEE Trans. Power App. Systems*, vol. PAS-101, no. 7, pp.1888-1893, Jul.1982
- [25] L. Q. Nguyen and B. Paradis, "Installation of Hydro Quebec's Distribution Feeder Automation System," *IEEE Trans. Power Del*, vol.3, no.4, pp. 1935-1941, Oct. 1988
- [26] T.P. Wagner, A.Y. Chikhani, and R. Hackam, "Feeder reconfiguration for loss reduction: An application of distribution automation," *IEEE Trans. Power Del*, vol. 6, no.4, pp. 1922-1933, Oct. 1991
- [27] Y. Matsumoto, T. Oohashi, and Y. Matsuura, "The concept of distribution automation system in the KANSAI Electric Power Co," in Proc. *IEEE PESW '99*, pp. 850-853, 1999.
- [28] EPRI, "Technical and System Requirements for Advanced Distribution Automation", Tech.Rep. TR-1010915, 2004.
- [29] Canadian Standards Association, "CAN3-C235-83 (R2010) – Preferred Voltage Levels for AC Systems, 0 to 50 000V," 1983
- [30] BC Hydro, "Distribution Standards – Overhead Electrical ES43 Series", Feb. 2002
- [31] WorkSafeBC, "Minimum separation distance to be maintained from energized high voltage electrical equipment and conductors", Part 19, Sections 19.24.1 and 19.24.2, 2011

- [32] IEEE 802.16-2004, "IEEE Standard for Local and Metropolitan Area Networks Part 16:Air Interface for Fixed Broadband Wireless Access Systems," Jul. 2004
- [33] WiMAX Forum. [Online]. Available: www.wimaxforum.org
- [34] IEEE 802.15.4, "Part 15.4: Wireless Medium Access Control (MAC) and Physical Layer (PHY) Specifications for Low Rate Wireless Personal Area Networks (WPAN)," 2009
- [35] Zigbee Alliance. [Online]. [Available]: www.zigbee.org
- [36] W. Webb, "Broadband fixed wireless access as a key component of the future integrated communications environment," *IEEE Commun. Mag.*, vol. 39, no. 9, pp. 115-121, Sep. 2001.
- [37] K. Lu, Y. Quian and H-H Chen, "Wireless broadband access: WIMAX and beyond," *IEEE Commun. Mag.*, vol. 45, no. 5, pp. 124-130, May 2007.
- [38] S. S. Venkata, . Pahwa, R. E. Brown, and R. D. Christie, "What future distribution engineers need to learn," *IEEE Trans. Power Syst.*, vol.19, no.1, pp. 17-23, Feb. 2004.
- [39] S. Jim, W. Carr, and S. E. Collier, "Real time distribution analysis for electric utilities," in *Proc. IEEE REPC'08*, pp. B5-B5-8, 27-29 Apr. 2008.
- [40] D. G. Michelson, V. Erceg, L. J. Greenstein, "Modeling diversity reception over narrowband fixed wireless channels," in *Proc. IEEE MTT-TWA'99*, pp. 95-100, 21-24 Feb. 1999.
- [41] L. J. Greenstein, S. S. Ghassemzadeh, V. Erceg and D. G. Michelson, "Ricean K-factors in narrowband fixed wireless channels: Theory, experiments and statistical models," in *Proc. WPMC'99*, 21-23 Sep. 1999.
- [42] S. Perras and L. Bouchard, "Fading characteristics of RF signals due to foliage in frequency bands from 2 to 60 GHz," in *Proc. WPMC'02*, 27-30 Oct. 2002, pp. 267-271.
- [43] M. J. Gans, N. Amitay, Y. S. Yeh, T. C. Damen, R.A. Valenzuela, C. Cheon and J. Lee, "Propagation measurements for fixed wireless loops (FWL) in a suburban region with foliage and terrain blockages," *IEEE Trans. Wireless Commun.*, vol. 1, no.2, pp. 302-310, Apr. 2002
- [44] E. R. Pelet, J. E. Salt, and G. Wells, "Effect of wind on foliage obstructed line-of-sight channel at 2.5 GHz," *IEEE Trans. Broadcasting*, vol. 50, no. 3, pp. 224-232, 2004.
- [45] D. Crosby, V. S. Abhayawardhana, I. J. Wassell, M. G. Brown, and M. P. Sellars, "Time variability of the foliated fixed wireless access channel at 3.5 GHz," in *Proc. IEEE VTC 2005 Spring*, 25-28 Sep. 2005, pp. 106-110.
- [46] R. Feick, R. A. Valenzuela and L. Ahumada, "Experiment results on the level crossing rate and average fade duration for urban fixed wireless channels," *IEEE Trans. Commun.*, vol. 9, no. 1, pp. 175-179, Jan. 2007.
- [47] H. Suzuki, C. D. Wilson, and K. Ziri-Castro, "Time variation characteristics of wireless broadband channel in urban area," presented at *EuCAP'06*, Nice, France, 2-6 Nov. 2006.

- [48] Industry Canada, "Policy for the Use of 700 MHz Systems for Public Safety Applications and Other Limited Use of Broadcasting Spectrum," Radio System Policy RP-006, Issue 1, Jun. 2006
- [49] Y. H. Lee and Y. S. Meng, "Tropical weather effects on foliage propagation," in *Proc. EuCAP '07*, pp. 1-5, Nov. 2007
- [50] L. J. Greenstein, D. G. Michelson, and V. Erceg, "Moment-method estimation of the Ricean K-factor," *IEEE Commun. Lett.*, vol. 3, no. 6, pp. 175-176, Jun. 1999.
- [51] D. S. Baum, D. A. Gore, R. U. Nabar, S. Panchanathan, K.V.S. Hari, V. Erceg and A. J. Paulraj, "Measurements and characterization of broadband MIMO fixed wireless channels at 2.5 GHz," in *Proc. IEEE ICPWD '00*, 17-20 Dec. 2000, pp. 203-206
- [52] S. R. Hanna and J. C. Chang, "Representativeness of wind measurements on a mesoscale grid with station separations of 312 m to 10 km," *Boundary-Layer Meteorol.*, vol. 60, pp. 309-324, 1992.
- [53] D. A. J. Pearce, A. G. Burr and T. C. Tozer, "Modelling and predicting the fading performance of fixed radio links through vegetation," in *Proc. IEE NCAP '99*, 31 Mar.-1 Apr. 1999, pp. 263-266.
- [54] P. Lédl, P. Pečač and M. Mazánek, "Time-series prediction of attenuation caused by trees for fixed wireless access systems operating in millimeter waveband," in *Proc. IEE ICAP '03*, 31 Mar.-3 Apr. 2003, pp. 646-649.
- [55] M. Cheffena and T. Ekman, "Modeling the dynamic effects of vegetation on radiowave propagation," in *Proc. IEEE ICC '08*, 19-23 May 2008, pp. 4466-4471
- [56] V. Erceg, K.V.S. Hari, et al., "Channel models for fixed wireless applications," Tech. Rep, IEEE 802.16 Broadband Wireless Access Working Group, Jan. 2001.
- [57] S. R. Saunders, *Antennas and Propagation for Wireless Communication Systems*. John Wiley & Sons Ltd, 1999.
- [58] S. R. Saunders and F. R. Bonar, "Mobile radio propagation in built-up areas: a numerical model of slow fading", in *Proc. IEEE VTC 1991 Fall*, pp. 295-300, 1991.
- [59] C. Chrysanthou and H. L. Bertoni, "Variability of sector averaged signals for UHF propagation in cities," *IEEE Trans. Veh. Tech.*, vol. 39, no. 4, pp 352-358, 1990.
- [60] M. Hata, "Empirical formula for propagation loss in land mobile radio services," *IEEE Trans. Veh. Technol.*, vol. 29, no. 3, pp. 317-325, Aug. 1980.
- [61] E. Damosso, Ed., "Digital Mobile Radio Toward Future Generation Systems – Final Report," COST 231 Final Report, 1996.
- [62] F. Fuschini, V. Degli-Esposti, and G. Falciasecca, "A statistical model for over rooftop propagation," *IEEE Trans. Antennas Propagat.*, vol. 52, no. 1, pp. 230-239, Jan. 2004.

- [63] K. Konstantinou, S. Kang and C. Tzaras, "A Measurement-Based Model for Mobile-to-Mobile UMTS Links," Center for Communication Systems Research, 2007.
- [64] S. R. Saunders, *Antenna and Propagation for Wireless Communication Systems*, John Wiley & Sons, Inc., New York, 1999.
- [65] M. Gudmundson, "Correlation model for shadow fading in mobile radio systems," *Elect. Lett.*, vol. 27, no.23, pp. 2145-46, Nov. 1991.